

AEDC-TR-92-5

AD - A255972

# Effects of Cryocontaminants on Cryogenic Superpolished Mirror and Quartz Crystal Microbalance

B. L. Seiber, R. J. Bryson, R. P. Young, Sr.,  
and B. E. Wood  
Calspan Corporation/AEDC Operations

September 1992

Final Report for Period March 1991 – December 1991

Approved for public release; distribution is unlimited.

**ARNOLD ENGINEERING DEVELOPMENT CENTER  
ARNOLD AIR FORCE BASE, TENNESSEE  
AIR FORCE MATERIEL COMMAND  
UNITED STATES AIR FORCE**

## NOTICES

When U. S. Government drawings, specifications, or other data are used for any purpose other than a definitely related Government procurement operation, the Government thereby incurs no responsibility nor any obligation whatsoever, and the fact that the Government may have formulated, furnished, or in any way supplied the said drawings, specifications, or other data, is not to be regarded by implication or otherwise, or in any manner licensing the holder or any other person or corporation, or conveying any rights or permission to manufacture, use, or sell any patented invention that may in any way be related thereto.

Qualified users may obtain copies of this report from the Defense Technical Information Center.

References to named commercial products in this report are not to be considered in any sense as an endorsement of the product by the United States Air Force or the Government.

This report has been reviewed by the Office of Public Affairs (PA) and is releasable to the National Technical Information Service (NTIS). At NTIS, it will be available to the general public, including foreign nations.

## APPROVAL STATEMENT


This report has been reviewed and approved.



SETH D. SHEPHERD, Capt, USAF  
Flight Dynamics Division  
Directorate of Technology  
Deputy for Operations

Approved for publication:

FOR THE COMMANDER



KEITH L. KUSHMAN  
Director of Technology  
Deputy for Operations

REPORT DOCUMENTATION PAGE			Form Approved OMB No. 0704-0188	
Public reporting burden for this collection of information is estimated to average 1 hour per response, including the time for reviewing instructions, searching existing data sources, gathering and maintaining the data needed, and completing and reviewing the collection of information. Send comments regarding this burden estimate or any other aspect of this collection of information, including suggestions for reducing this burden, to Washington Headquarters Services, Directorate for Information Operations and Reports, 1215 Jefferson Davis Highway, Suite 1204, Arlington, VA 22202-4302, and to the Office of Management and Budget, Paperwork Reduction Project (0704-0188), Washington, DC 20503.				
1. AGENCY USE ONLY (Leave blank)	2. REPORT DATE September 1992	3. REPORT TYPE AND DATES COVERED Final - March - December 1991		
4. TITLE AND SUBTITLE  Effects of Cryocontaminants on Cryogenic Superpolished Mirror and Superpolished Quartz Crystal Microbalance		5. FUNDING NUMBERS  PE - 921F01 PR - DC95VK		
6. AUTHOR(S)  Seiber, B. L., Bryson, R. J., Young, R. P., Sr., and Wood, B. E., Calspan Corporation/AEDC Operations				
7. PERFORMING ORGANIZATION NAME(S) AND ADDRESS(ES)  Arnold Engineering Development Center/DOT Air Force Systems Command Arnold Air Force Base, TN 37389-5000		8. PERFORMING ORGANIZATION REPORT NUMBER  AEDC-TR-92-5		
9. SPONSORING/MONITORING AGENCY NAME(S) AND ADDRESS(ES) Rome Laboratory Griffiss Air Force Base, NY and Johns Hopkins Applied Physics Laboratory Laurel, MD		10. SPONSORING/MONITORING AGENCY REPORT NUMBER		
11. SUPPLEMENTARY NOTES  Available in Defense Technical Information Center (DTIC).				
12a. DISTRIBUTION/AVAILABILITY STATEMENT  Approved for public release; distribution is unlimited.		12b. DISTRIBUTION CODE		
13. ABSTRACT (Maximum 200 words)  Effects of contaminants on optical surfaces is a concern for space-based systems. Many systems contain cryogenic optical systems that operate at temperatures where gases such as nitrogen, oxygen, carbon dioxide, and water will condense. This study presents experimental results of the effects of these gases condensed on highly polished (superpolished) mirror surfaces cooled, under vacuum, to temperatures as low as 15 K. Using these gases as contaminants, the bidirectional reflectance distribution function (BRDF) was obtained at a wavelength of 0.6328 $\mu\text{m}$ for various contaminant film thicknesses up to 8 $\mu\text{m}$ . Most of the data were obtained using the superpolished sense crystal of a previously developed quartz crystal microbalance (SPQCM) as the mirror surface.  The SPQM allowed the mass of the actual contaminant layer to be measured directly. This program has been sponsored by Rome Laboratory and Johns Hopkins University Applied Physics Laboratory.				
14. SUBJECT TERMS BRDF cryocontaminant		superpolished mirror quartz crystal microbalance		15. NUMBER OF PAGES 66
				16. PRICE CODE
17. SECURITY CLASSIFICATION OF REPORT UNCLASSIFIED	18. SECURITY CLASSIFICATION OF THIS PAGE UNCLASSIFIED	19. SECURITY CLASSIFICATION OF ABSTRACT UNCLASSIFIED	20. LIMITATION OF ABSTRACT SAME AS REPORT	

## **PREFACE**

The work reported herein was performed by the Arnold Engineering Development Center (AEDC), Air Force Systems Command (AFSC) under Program Element 921F01, Control Number 9F01. The results were obtained by Calspan Corporation, AEDC Operations, support contractor for Aerospace Flight Dynamics testing at AEDC, AFSC, Arnold Air Force Base, Tennessee, under AEDC Project Number DC95VK. The project was sponsored by Rome Laboratory (RL) Rome, New York and Johns Hopkins Applied Physics Laboratory (JHU/APL), Laurel, Maryland. Project Managers were Capt. Deidra Dykeman (RL), Dr. Manuel Uy (JHU/APL), and Capt. Seth Shepherd (AEDC/DOT). The manuscript was submitted for publication on August 13, 1992.

The authors would like to thank Bill Hobbs and Winfred Johnson for their help with the Bidirectional Reflectance Distribution Function (BRDF) chamber operation and instrumentation.

## CONTENTS

	<u>Page</u>
1.0 INTRODUCTION .....	5
2.0 EXPERIMENTAL TEST APPARATUS .....	5
2.1 BRDF Chamber .....	5
2.2 BRDF Measuring Apparatus .....	6
2.3 Test Mirrors .....	7
2.4 Quartz Crystal Microbalance (QCM) .....	8
2.5 Gas Addition System .....	9
2.6 Film Thickness Apparatus .....	10
2.7 Data Acquisition Systems .....	10
3.0 EXPERIMENTAL TEST PROCEDURE .....	11
3.1 Superpolished Mirror Preparation .....	11
3.2 Superpolished QCM (SPQCM) Preparation .....	11
3.3 Gas Addition System Preparation .....	12
3.4 BRDF Measurement .....	12
3.5 Film Thickness Calculation .....	15
3.6 Deposit Density Determination .....	15
3.7 Contamination Test .....	16
4.0 RESULTS AND DISCUSSION .....	17
4.1 Superpolished Mirror Data .....	17
4.2 SPQCM Data .....	18
4.3 Data Uncertainty .....	23
5.0 CONCLUDING REMARKS .....	27
REFERENCES .....	28

## ILLUSTRATIONS

<u>Figure</u>	<u>Page</u>
1. BRDF Test Chamber .....	31
2. Exploded View of the Mark 16 .....	33
3. SSG Superpolished Mirror Degradation at Selected CO <sub>2</sub> Film Thickness; 40 K Surface, 0.6328 $\mu\text{m}$ .....	34
4. SSG Superpolished Mirror Degradation at Selected H <sub>2</sub> O Film Thickness; 40 K Surface, 0.6328 $\mu\text{m}$ .....	35
5. SPQCM Degradation at Selected N <sub>2</sub> Film Thickness; 15 K Surface, 0.6328 $\mu\text{m}$ .....	36

FigurePage

6. SPQCM 5-deg BRDF Change with N <sub>2</sub> Contamination; 15 K Surface, 0.6328 $\mu\text{m}$ .....	37
7. Linearity of SPQCM Frequency with Nitrogen Film Thickness .....	38
8. SPQCM Degradation at Selected O <sub>2</sub> Film Thickness; 25 K Surface, 0.6328 $\mu\text{m}$ .....	39
9. SPQCM with O <sub>2</sub> Contamination; 15 K Surface, 0.6328 $\mu\text{m}$ .....	41
10. Linearity of SPQCM Frequency Change with Oxygen Film Thickness .....	43
11. Warmup of SPQCM Crystal with O <sub>2</sub> Contaminant; 15 K Surface, 0.6328 $\mu\text{m}$ .....	44
12. SPQCM Degradation at Selected CO <sub>2</sub> Film Thickness, 0.6328 $\mu\text{m}$ .....	47
13. SPQCM with CO <sub>2</sub> Contamination; 20 K Surface, 0.6328 $\mu\text{m}$ .....	49
14. Linearity of SPQCM Frequency with CO <sub>2</sub> Film Thickness .....	51
15. SPQCM Degradation at Selected H <sub>2</sub> O Film Thickness; 27 K Surface, 0.6328 $\mu\text{m}$ .....	52
16. SPQCM 6-deg BRDF Change with H <sub>2</sub> O Contamination; 27 K Surface, 0.6328 $\mu\text{m}$ .....	53
17. Change in 6-deg BRDF with SPQCM Warmup; H <sub>2</sub> O Contaminant, 27 K Surface, 0.6328 $\mu\text{m}$ .....	54
18. SPQCM Degradation with Film Layers, N <sub>2</sub> then CO <sub>2</sub> ; 16 K Surface, 0.6328 $\mu\text{m}$ .....	55
19. SPQCM 6-deg BRDF Change with N <sub>2</sub> , then CO <sub>2</sub> Contamination Layers; 15 K Surface, 0.6328 $\mu\text{m}$ .....	56
20. Linearity of SPQCM with Layered Film Thickness, N <sub>2</sub> then CO <sub>2</sub> .....	57
21. Change in 6-deg BRDF with SPQCM Warmup; Contaminant, Layered CO <sub>2</sub> over N <sub>2</sub> , 15 K Surface, 0.6328 $\mu\text{m}$ .....	58
22. SPQCM Degradation with Film Layers, CO <sub>2</sub> then N <sub>2</sub> ; 15 K Surface, 0.6328 $\mu\text{m}$ .....	59
23. SPQCM 6-deg BRDF Change with CO <sub>2</sub> then N <sub>2</sub> Contamination Layers; 15 K Surface, 0.6328 $\mu\text{m}$ .....	60
24. Change in 6-deg BRDF with SPQCM Warmup; Contaminant, Layered N <sub>2</sub> over CO <sub>2</sub> , 15 K Surface, 0.6328 $\mu\text{m}$ .....	61
25. SPQCM Degradation with Film Thickness; Mixed Gas with Equal Parts N <sub>2</sub> , O <sub>2</sub> , and CO <sub>2</sub> ; 16 K Surface, 0.6328 $\mu\text{m}$ .....	62
26. SPQCM 6-deg BRDF Change with Mixed Gas Contamination, Equal Parts N <sub>2</sub> , O <sub>2</sub> , and CO <sub>2</sub> ; 16 K Surface, 0.6328 $\mu\text{m}$ .....	63

## 1.0 INTRODUCTION

This report describes the effects of contaminant films on the reflecting properties of highly polished optical surfaces. For sensor systems which contain optical surfaces maintained at cryogenic temperatures, a major concern is that low-temperature contaminant films can condense on the mirror surface, which alters the reflective properties. The property of most concern is the bidirectional reflectance distribution function (BRDF). BRDF describes the radiation that is scattered by the mirror into directions other than the specular. The BRDF is the major factor in determining whether optical systems are capable of differentiating a weak target source in the vicinity of a much stronger one.

In this study, contaminant films were condensed on highly polished mirror surfaces of two types. One surface was a conventional highly polished mirror that was provided by SSG, Inc. of Waltham, MA. The other surface was that of a superpolished quartz crystal microbalance (SPQCM) that had been developed through a program with QCM Research Company of Laguna Beach, CA. Both surfaces were cooled to temperatures as low as 16 K, although some measurements were made at temperatures as high as 48 K.

The contaminant films investigated were water, nitrogen, oxygen, carbon dioxide, and mixtures comprised of those constituents. The film thicknesses were determined using a thin-film interference technique and ranged from zero to approximately 10- $\mu\text{m}$  thick. The scatter, or BRDF, was measured using a He-Ne laser that operated at 0.6328  $\mu\text{m}$ . This study was the first portion of a BRDF measurements program that will include measurements at 10.6 and 3.39  $\mu\text{m}$  in the next phase. The next phase will also include BRDF measurements on contaminant films derived from the outgassing products of satellite materials.

## 2.0 EXPERIMENTAL TEST APPARATUS

### 2.1 BRDF CHAMBER

The BRDF chamber provides a technique for measuring the changes in the BRDF of a superpolished test surface as it is contaminated by condensed gases. The equipment allows introduction of contaminant gas or the generation of outgassing products within the chamber. Determination of the mass of material deposited is accomplished using a QCM. The thickness of the material is determined by counting the 0.6328- $\mu\text{m}$  laser interference fringes as the contamination layer is deposited. For the current measurements, various gases were condensed on mirror surfaces which were either a superpolished plane mirror or a SPQCM, and the BRDF was measured at 0.6328  $\mu\text{m}$ . The BRDF Test Chamber and associated BRDF equipment are shown in Fig. 1. The details of these systems are discussed separately in the following sections.

The BRDF Test Chamber vacuum is maintained by a turbomolecular pump. The chamber is also outfitted with a liquid-nitrogen-cooled liner and a gaseous helium-cooled scavenger panel. The pressure in the chamber is measured with a Bayard-Alpert-type ion gage and can be maintained below  $10\text{E}-7$  torr when the contaminant gas load is small.

In addition to the scavenger panel, gaseous helium was used to cool the BRDF measurement sample and the QCM. The ultimate cryogenic temperature for the reflectance sample depended on the sample mounting configuration and on the refrigerator performance. Temperatures as low as 15 K have been obtained.

## 2.2 BRDF MEASURING APPARATUS

The BRDF apparatus and measurement followed the technique described by Young (Ref. 1). The BRDF measurement apparatus consisted of a laser and beam shaping optics exterior to the chamber. Inside the chamber, the laser beam irradiated the superpolished mirror surface at a near-normal angle of incidence (less than 2 deg). A detector assembly mounted on a computer-controlled rotary arm was used to measure the scattered light intensity as a function of the scattering angle. The system was calibrated using a barium sulfate diffuse scattering sample in place of the test mirror.

The laser was a 12-mW helium-neon laser operating at  $0.6328\ \mu\text{m}$  with a randomly polarized beam. The beam power could be periodically measured with a radiometer inserted in the beam to check for laser intensity drift between diffuser and the test mirror measurements.

The beam shaping optics consisted of a lens-pinhole-spatial filter followed by a focusing lens which illuminated a 6-mm central spot on the test mirror and, in the specular direction, imaged the pinhole of the spatial filter on the entrance aperture of the detector. To reduce the stray scattered light, a sequence of apertures was located inside the chamber. This reduced the effects of the scattered light from the optics and the chamber window.

The detector assembly consisted of a lens that projected an image of the illuminated portion of the test mirror on a  $1\text{-mm}^2$  silicon detector. This reduced the contribution of unwanted stray light on the detector. The detector and lens were fastened together in a gimbal mount, allowing the detector to be centered on the image of the illuminated portion of the test mirror. The detector assembly also contained a remotely operated shutter with different apertures. The entire assembly (detector, lens, shutter, and gimbal) was mounted to one end of an arm, the opposite end of which was fastened to a computerized, motor-driven rotary table. The rotary arm assembly had a resolution on the order of 0.002 deg.



A diffuser consisting of barium sulfate of known reflectance characteristics (Ref. 2) was mounted near the test mirror. This diffuser could be moved into position, when needed, to calibrate the system.

The detector signal passed through a preamplifier to a lock-in amplifier which was read by computer. With computer control, the measurement system had the capability of making scattering measurements at preprogrammed angles by moving the detector to a prescribed angle, reading the detector output, then moving to the next angle, etc.

Much of the stray light scattered off of the entrance window and optics exterior to the BRDF chamber was removed by a sequence of apertures through which the laser beam passed. To limit the detector field-of-view, improving the stray light rejection, a telescope was attached to the detector assembly. The telescope imaged the detector on the illuminated area of the sample mirror. In principle, only the light that enters the telescope lens and originates from the portion of the sample surface covered by the detector image will be measured by the detector. In practice, a small portion of the light from other sources that enters the telescope may be scattered by the telescope imperfections into the detector. Even with imperfections, the telescope prevented a large portion of the stray light from reaching the detector. The laser beam was Gaussian in profile with visible energy up to 2 cm from the central spot on the sample mirror. A portion of the laser light could be reflected back toward the detector by the sample mount or the SPQCM housing. A black mask with a 1-cm aperture was placed over the mirror and SPQCM samples. This made an order-of-magnitude improvement in the stray light at large angles (30 deg) with the SPQCM. Another source of stray radiation peculiar to the BRDF chamber installation was the reflection of the laser beam from the specular beam detector used for the thickness measurement. Care was taken when mounting this detector to make certain that the specular reflection from this specular detector passed into the beam dump. A final source of scattered light was reflections from the BRDF detector mount when the detector was set at angles near specular (less than approximately 3 deg).

### 2.3 TEST MIRRORS

Two types of test mirrors were used, a superpolished mirror and a SPQCM. The superpolished mirror was a 2.5-cm (1.0 in.)-diam, nickel, plane mirror supplied by SSG Inc. The mirror was finished to provide a low scatter surface using a proprietary process. Temperature sensors and a foil resistance heater with Kapton insulation were mounted to the mirror backside. The unit was mounted in an aluminum block which could be cooled by flowing gaseous helium through it. The conduction path for cooling the mirror was through the resistance heater to the aluminum cooling block. To monitor the mass deposited on the mirror, a conventional QCM (not superpolished) was mounted in the cooling block adjacent to the mirror.

The SPQCM was used as the test mirror for most of the measurements. The SPQCM was a Mark 16 QCM manufactured by QCM Research that had been customized by the installation of a set of aluminum overcoated superpolished quartz crystals. The SPQCM was one of two supplied by QCM Research on a development contract funded by Rome Laboratory.

## 2.4 QUARTZ CRYSTAL MICROBALANCE (QCM)

For the superpolished mirror measurements, the deposition monitoring QCM was mounted in the cooled block next to the superpolished mirror with the intention that they would be at the same temperature and encounter the same gas load. In practice, equal temperatures were difficult to obtain, and the geometry was not identical. This resulted in different gas loads on the superpolished mirror and the QCM; the differences being difficult to quantize. The problem was solved by using the SPQCM, which combined the important attributes of the QCM and the superpolished mirror. Since the measurements of mass, BRDF, and film thickness were made on the same surface, the problem of different gas loads was eliminated.

A QCM is based on the principle that the oscillation frequency of a quartz crystal varies proportionally to its mass or any mass adhering to the crystal surface. The oscillation frequency is also dependent on other things such as temperature. To compensate for temperature effects, the QCMs are made up of two quartz crystal oscillators in a single housing (Fig. 2). The oscillator outputs are mixed, and their difference frequency is monitored. One crystal oscillator (the reference oscillator) is enclosed and shielded from contaminants, seeing temperature effects but not contaminants. One surface of the other quartz crystal oscillator is polished to an optical finish and overcoated with aluminum. It is exposed to the contaminant flow and is used as the mass-sensing oscillator. The change between the two oscillator frequencies, (i.e., the change in the difference frequency) is attributed to the accumulated mass from the contaminant.

The relation between the difference frequency change,  $df$ , and the deposited mass change,  $dm$ , can be expressed as (Refs. 3 and 4)

$$dm/A = C df \quad (1)$$

where  $A$  is the surface area of the sensing crystal exposed to deposits. The value of  $C$  is determined from

$$C = PV/(2F^2) \quad (2)$$

where

F is the fundamental frequency of the quartz crystal, Hz

P is the quartz density ( $2.664 \text{ gm/cm}^3$ )

V is the shear wave velocity ( $3.3713 \times 10^5 \text{ cm/sec}$ ) (Ref. 3).

For a standard 10-MHz crystal, then  $C = 4.49 \times 10^{-9} \text{ gm cm}^{-2} \text{ Hz}^{-1}$ .

The superpolished crystals used in this investigation were measured to have an oscillation frequency of 10.96 MHz. For the superpolished crystals used, C becomes  $C = 3.74 \times 10^{-9} \text{ gm cm}^{-2} \text{ Hz}^{-1}$ .

The Mark 16 QCM (Fig. 2) has a silicon temperature sensor mounted between the sensing and reference crystals to monitor the crystal temperature. To warm the crystal pack independent of the QCM housing mount temperature, the crystal pack is isolated from the base and mount by small tubular supports, and the crystal pack has a 3-W resistance heater mounted to it. This combination allows the crystals to be kept warm until ready to condense contaminants. A thermogravimetric analysis (TGA) can be accomplished by warming the crystals, evaporating the cryofilm, and noting at what temperatures the previously condensed gases evaporate.

The QCM Research model 1819 controller was capable of supplying oscillator and heater power for up to four Mark 16 QCMs and outputting the oscillator difference frequency, crystal pack temperature, accumulated mass, and mass rate on the sense crystal. The controller could be programmed to heat the crystal pack to a temperature at a specified rate.

As installed, an external power supply was used for the QCM oscillators. This allowed convenient adjustment of the operating voltage. In addition, a preamplifier was installed in the QCM oscillator line between the QCM head and the controller. This preamplifier boosted the signal level above the threshold required by the frequency counter and reduced problems of spurious noise causing changes in the measured frequency. To monitor the QCM performance, a breakout box was installed in the QCM cable between the QCM head and the controller. The breakout box allowed data system recording of the oscillator supply voltage and current, the QCM heater voltage and current, and the QCM crystal pack temperature.

## 2.5 GAS ADDITION SYSTEM

The gas addition system introduced the desired gases into the chamber for deposition on the superpolished samples. The system consisted of a contaminant gas source, a metering

valve, and an injection tube inside the BRDF chamber that directed the gas flow in the direction of the superpolished sample. The contaminant sources were the purified gases carbon dioxide, oxygen, and nitrogen which were stored in pressurized steel bottles. The source for water vapor was a glass vial of water that was valved into the gas addition system so that only the gas phase above the liquid was introduced. The metering valve was an adjustable vacuum leak valve that was used to obtain a convenient deposition rate on the superpolished sample. The injection tube was 6-mm-diam stainless-steel tubing protruding 60 cm into the chamber so that the superpolished sample surfaces were located in the gas plume exiting the injection tube.

## 2.6 FILM THICKNESS APPARATUS

A portion of the BRDF apparatus was used to measure the cryofilm thickness. As the gas was deposited on the superpolished sample surface, the specular component of the He-Ne laser beam reflected from the superpolished sample was monitored with a silicon solar cell. For stray light reduction, the specular laser beam was captured by a beam dump mounted on the chamber wall. The thin wafer silicon solar cell (2 cm by 8 cm) was mounted in the beam dump. Care was taken to locate the solar cell so the specular reflection from its surface did not exit the beam dump. The electrical signal from the solar cell was amplified, rectified, and recorded on a strip chart.

The reflected specular intensity variation with deposit thickness is described by thin-film interference theory. As the cryofilm thickness increases, the signal from the specular beam passes through maxima and minima. The thickness of the cryofilm,  $t$ , is determined from the thin-film interference equation for reflection maxima (Ref. 5):

$$t = \frac{mL}{2n\sqrt{1 - \frac{\sin^2 \theta}{n^2}}} \quad (3)$$

where  $m = 1, 2, 3, \dots$ ,  $L$  is the spectral wavelength of the laser radiation,  $\theta$  is the incidence angle of the radiation measured from the normal, and  $n$  is the real component of the refractive index of the deposit. The thickness and wavelength are expressed in the same units, often micrometers and the other two quantities,  $m$  and  $n$ , are unitless.

## 2.7 DATA ACQUISITION SYSTEMS

The BRDF scattering measurements were recorded and reduced on the personal computer that controlled the BRDF apparatus. The thickness-related specular intensity information

was recorded on a strip chart that monitored the maxima associated with the cryofilm. All other data were recorded on a separate system used for general housekeeping.

The housekeeping data system was based on a microcomputer tied by serial communication lines to several data units. A 64-channel data logger was used to read the analog data channels such as chamber pressures, temperatures from thermocouples, and the QCM oscillator and heater voltages. An 8-channel readout for silicon diode temperature sensors was used to obtain temperatures of the cryopanel and the mounting block for the superpolished sample. The QCM controller was used to obtain the QCM frequency and temperature. At intervals set in the data logger, such as one minute, the microcomputer obtained data from the data logger and the remaining devices. In addition, when desired, the fixed angle scattering intensity from the BRDF scattering apparatus was also obtained. These data were displayed on a video terminal, printed, and recorded on a hard disk. The data were later reduced and plotted using various computers.

### **3.0 EXPERIMENTAL TEST PROCEDURE**

Initially, the superpolished mirror obtained from SSG was installed, and scattering measurements were made using carbon dioxide and water vapor as the contaminating source gases. Later, the SPQCM was installed and because of its previously stated advantages, all of the remaining scattering measurements were made on the SPQCM.

#### **3.1 SUPERPOLISHED MIRROR PREPARATION**

On receipt, the BRDF of the superpolished mirror was measured in a clean room environment then covered with a metal cap until ready for use. This measurement was used as a baseline to evaluate the deterioration of the mirror BRDF with use.

A foil resistance heater and platinum resistance temperature sensor were bonded to the back of the mirror prior to installation in a helium-cooled mounting block in the BRDF chamber. This allowed limited heating of the mirror for deposit removal. The mirror was kept covered when not in use, the cover being removed just before closing the chamber. The mirror cover was reinstalled on chamber opening.

#### **3.2 SUPERPOLISHED QCM (SPQCM) PREPARATION**

As with the superpolished mirror, the BRDF of the superpolished quartz sensing crystal was measured in a clean room environment on receipt. A metal cap was then used to protect it from contaminating particles.

Prior to installation of the SPQCM, the BRDF chamber was vacuumed and wiped to reduce chamber particles as much as possible. To further minimize dust contamination, the vacuum chamber pressure excursions were kept to a minimum, the chamber brought slowly to atmosphere, and the SPQCM covered when the chamber was opened. To minimize scattered radiation from bright metallic, non-optical portions of the SPQCM, a flat black mask with a 9.5-mm (0.38 in.) aperture was installed on the cooling block in front of the SPQCM.

### 3.3 GAS ADDITION SYSTEM PREPARATION

Contamination gases were supplied to the chamber by connecting the desired gas bottle to the gas addition system. The lines up to the gas bottle were evacuated by the vacuum system to remove trapped gas. When ready for gas addition, the lines were valved to the chamber, and the leak valve was opened until the desired flow rate was obtained. The flow rate indication was taken from the QCM frequency shift and the change in the interference fringe maxima and minima.

For water vapor addition, the procedure was slightly different. The glass water vapor flask was partially filled with water and partially evacuated with a vacuum pump to remove most of the air. The flask with a partial vacuum was then valved shut. The flask was attached to the gas addition system and the lines were evacuated, as with the bottled gas, to remove entrapped air. During water addition, the temperature of the gas injection tube was monitored and heat was added to the injection tube as necessary to keep the water in the gas phase.

### 3.4 BRDF MEASUREMENT

#### 3.4.1 BRDF Method

The concept of BRDF was introduced by Nicodemus (Ref. 6) under the name partial reflectance, then renamed to the current usage, BRDF, in Ref. 7. The definition and geometrical concepts of BRDF are extensively covered using current terminology in Ref. 8. Nicodemus defined the BRDF of an opaque, reflective surface in terms of the incident irradiance,  $E_i$  ( $\text{W}/\text{m}^2$ ), and the reflected radiance,  $L_r$  ( $\text{W m}^{-2} \text{sr}^{-1}$ ), in the differential form

$$\text{BRDF} = dL_r/dE_i, \text{ sr}^{-1} \quad (4)$$

In general, the BRDF of a reflecting surface is a function of the direction of the incident radiation and the direction of the reflected or scattered radiation. The BRDF definition is for an infinitely small surface area and solid angles of incident and reflected radiation. Experimental BRDF measurements involve finite area and solid angles. This results in a measured BRDF value that is averaged over the finite quantities used.

For the BRDF measurement of a surface in the BRDF chamber, the direction of the incident radiation was near normal to the reflecting/scattering surface. The reflected/scattered radiation was measured with a detector assembly mounted to an arm that pivoted about an axis in the plane of the reflecting surface. The arm was rotated through different angles and the reflected radiation was measured (Fig. 1). Williams (Ref. 9) treated the BRDF calculation for a similar configuration and listed the simplifying assumptions for the measurement. Using these simplifying assumptions that small elements are used, the BRDF can be expressed in the following form

$$\text{BRDF}(\theta) = L_r(\theta)/E_i, \text{sr}^{-1} \quad (5)$$

where  $\theta$  is the angle between the direction of the reflected radiation and the reflecting surface normal. The reflected radiation,  $P(\theta)$ , intercepted by the detector entrance aperture is given by the following expression:

$$P(\theta) = \frac{A_d A_s \cos(\theta) L_r(\theta)}{D^2}, \text{ W} \quad (6)$$

where

$A_d$  is the area of the detector aperture,  $\text{m}^2$

$A_s$  is the illuminated area of the sample surface,  $\text{m}^2$

$D$  is the distance from the center of the sample surface illuminated area to the detector entrance aperture,  $\text{m}$

$\theta$  is the reflecting/scattering angle measured between the direction of the reflected radiation and the reflecting surface normal ( i.e., the angle between the detector arm and the sample surface normal),  $\text{deg}$

$L_r$  is the radiance of the reflected radiation in the direction of the detector,  $\text{W m}^{-2} \text{sr}^{-1}$ .

This equation can be solved for  $L_r$  giving

$$L_r(\theta) = \frac{PD^2}{A_d A_s \cos(\theta)}, \text{ W m}^{-2} \text{sr}^{-1} \quad (7)$$

Rather than measuring the incident radiation and the geometry factors, a reference reflector with known reflection/scatter characteristics can be interchanged with the sample surface. Two common choices are a specular reflector such as black glass or a diffusing reflector

that approximates a Lambertian surface (Ref. 8). Using Eq. (5) and Eq. (7), the following relation can be made between the BRDF and the power to the detector,

$$\text{BRDF}_s = \text{BRDF}_{\text{ref}} \left( \frac{P_s}{P_{\text{ref}}} \right) \left[ \frac{\cos(\theta_{\text{ref}})}{\cos(\theta_s)} \right], \text{ sr}^{-1} \quad (8)$$

where the notations (ref) and (s) refer to the reference and sample quantities. The reference surface for the BRDF chamber measurements was a barium sulfate diffusing surface (Ref. 2). Barium sulfate has a reflectivity of 0.98 at 0.6328  $\mu\text{m}$  for near normal incidence and approximates a Lambertian surface. For near normal incidence and reflection angles, the BRDF for the barium sulfate diffusing surface would be constant (Ref. 8) given by

$$\text{BRDF}_{\text{ref}} = 0.98/\pi. \quad (9)$$

One more assumption was required, that the detector output voltage (V) is proportional to the power incident on the detector entrance aperture. The final equation, the one used for the BRDF calculation, was

$$\text{BRDF}_s = 0.98(V_s/V_{\text{ref}})/(\pi \cos(\theta_s)), \text{ sr}^{-1}. \quad (10)$$

This was the same technique used by Young (Ref. 10).

### 3.4.2 Basic BRDF Measurement

The basic BRDF degradation measurement proceeded as follows:

1. The superpolished sample and the reference diffuser (barium sulfate surface) were installed in the BRDF chamber.
2. The BRDF chamber was closed and pumped down.
3. Under vacuum, the reference diffuser was inserted into the laser beam. The optics and detector were aligned, and several measurements were made of the scattered radiation near specular along with the laser output power. This was used as the scattering reference signal.
4. The superpolished sample mirror was inserted into the laser beam. The position of the specular reflection and the detector were adjusted so that the entrance aperture of the detector would be centered on the specular reflection when the detector arm was at an angle of 0-deg scattering angle (measured from specular). The laser output power and the detector output were measured as the detector



was stepped through set angles from 2 deg through 30 deg. This became the sample scattering signal.

5. The BRDF was calculated using the data obtained in steps 4 and 5.
6. Because of movement of the specular beam as the sample mounting block was cooled with gaseous helium, the alignment of the specular beam to the detector entrance aperture (step 4) was repeated when the mounting block was cold. Experience showed that the alignment did not change as long as the mounting block was at cryogenic temperatures.
7. A contaminant deposit was applied to the superpolished sample, the BRDF detector scan was made of the contaminated mirror, and the new BRDF was calculated.

### 3.5 FILM THICKNESS CALCULATION

As the contaminating gas was injected into the BRDF chamber, the interference fringe maxima were counted on a strip chart recorder. The gas addition system was shut off when the desired number of maxima were obtained. The film thickness was calculated using Eq. (3). The values used for the refractive index at 20 K (Refs. 5, 11) are listed below.

<u>Gas</u>	<u>Refractive Index</u>	<u>Thickness/Fringe</u>
Oxygen	1.25	0.253 $\mu\text{m}$
Nitrogen	1.26	0.251 $\mu\text{m}$
Carbon Dioxide	1.28	0.247 $\mu\text{m}$
Water	1.31	0.242 $\mu\text{m}$

### 3.6 DEPOSIT DENSITY DETERMINATION

The SPQCM with the interference fringe monitor allowed the density of the contaminant deposit to be determined. The SPQCM gave the mass per unit area of the deposit,  $\text{dm}/A$ , [Eq. (1)], and the interference fringes gave the thickness,  $t$ , [(Eq. (3))]. From these relations density was determined by the following:

$$\text{Density} = [\text{dm}/A]/t = C \, df/t, \text{ gm cm}^{-3} \quad (11)$$

where  $C = 3.74 \times 10^{-9} \text{ gm cm}^{-2}\text{Hz}^{-1}$ , for 10.96-MHz crystals in the SPQCM,  $df$  = QCM frequency change, Hz, and  $t$  = film thickness, cm.

As the contaminant gas was deposited on the QCM, the interference fringe intensity was recorded on the strip chart recorder. In addition, the QCM frequency was hand-recorded at the time the fringe maximum occurred. The average frequency change per fringe was used to calculate the density.

### **3.7 CONTAMINATION TEST**

#### **3.7.1 Superpolished Mirror**

The contamination tests with the superpolished mirror were conducted as follows. First, the BRDF chamber was evacuated, then when the chamber pressure was approximately  $10\text{E} - 5$  torr, the liquid-nitrogen liner was cooled to approximately 80 K and maintained at this temperature for the duration of the test. As the nitrogen liner approached its final temperature, the gaseous helium refrigerator was used to simultaneously cool the helium cryopanel in the top of the BRDF chamber and the mounting block for the superpolished mirror. The helium system was kept cold for the duration of the contamination test. In some cases, this lasted for more than one day. The superpolished mirror resistance heater was kept on until the gas contamination phase was started. Next, the mirror heat was turned off and as the mirror approached its final temperature in the vicinity of 40 K, a pre-contaminant BRDF scan was made. Then the contaminant gas was injected into the chamber until an interference maximum was obtained. The gas injection was turned off, and a BRDF scan was taken of the contaminated surface. The gas injection was restarted, and gas was added until the next interference maximum was reached. The gas was again turned off, and a BRDF scan was made. The process was repeated until the desired maximum thickness was obtained. For the cases where the desired thickness was not obtained in one day, the gas was shut off, a BRDF scan was taken, and the mirror was kept cold overnight. The following morning, the BRDF scan was repeated before the gas addition was continued. After the last BRDF scan, the mirror heater was turned on and the helium refrigerator was turned off and allowed to warm. After the helium system temperature was considerably above the nitrogen liner temperature, the nitrogen liner was allowed to warm. The object was to minimize additional contamination to the superpolished mirror as the helium panel and nitrogen panel dumped their cryogenic load. Arnold (Ref. 12) had encountered residue remaining after cryofilms had evaporated. This residue was removed by heating the surface above 330 K. These same effects were observed in these studies, so the superpolished mirror and QCM were heated to 340 K, which removed the remaining residue of contaminant.

#### **3.7.2 SPQCM**

The cooling procedure for the SPQCM phase was similar to that for the superpolished mirror, except that for the water and mixed gas contamination runs, a revised

helium refrigerator valving allowed the helium cryopanel to be cooled before the SPQCM mounting block. To reduce chances for unwanted contamination condensing on the SPQCM surface, the SPQCM heater was turned off last, and the gas addition was started as soon as the SPQCM reached the desired temperature. The SPQCM was kept at 340 K and under vacuum between tests.

## 4.0 RESULTS AND DISCUSSION

A superpolished mirror obtained from SSG, Inc. was installed in the BRDF chamber, and BRDF data were obtained for carbon dioxide and water contamination deposits with the superpolished mirror in the vicinity of 40 K. The SPQCM was then installed and BRDF scatter data were obtained for the following contamination gases condensed on the SPQCM: single gases of nitrogen, oxygen, carbon dioxide, and water; layered gases of nitrogen with a carbon dioxide overlay, and in reverse order, layered gases of carbon dioxide with a nitrogen overlay, and finally a mixture of equal parts nitrogen, oxygen, and carbon dioxide. Using the mass per unit area determined with the SPQCM and the thickness of the layer determined by the interference fringes, the average density of these condensed films was determined. Because of better thermal contact with its cooled mounting block, the SPQCM data were obtained in the 15 to 27 K range versus the 40 to 50 K temperature for the superpolished mirror. The differences in the SPQCM minimum temperature were caused by different helium refrigerator performance on different days.

All BRDF data were obtained at  $0.6328\ \mu\text{m}$  using a randomly polarized helium-neon laser. Also, all BRDF data presented are for angles measured from the direction of the specularly reflected ray.

### 4.1 SUPERPOLISHED MIRROR DATA

The superpolished mirror could only be cooled to a temperature near 40 K. With the BRDF chamber pressure approximately  $10\text{E}-7$  torr, the mirror was not cold enough to condense oxygen and nitrogen. Hence, BRDF data were only obtained for water and carbon dioxide. Because of the anticipated difficulty in removing water from the BRDF chamber, carbon dioxide data were taken first. These data are shown in Fig. 3 for selected thicknesses up to  $4\ \mu\text{m}$  where the gas addition was terminated. In addition to the film thickness, the interference fringe maximum number is shown for reference. No measurable change in the BRDF was noted for thicknesses less than  $0.49\ \mu\text{m}$ . For the larger thicknesses shown, the BRDF increased smoothly, with the contaminant film becoming increasingly more diffuse. The BRDF at large angles such as 30 deg increased more per film thickness increase than for small angles such as 5 deg. Notice also the smooth BRDF increase with contaminant film thickness for all angles.

The BRDF measurements of selected thicknesses of water films are shown in Fig. 4. For thicknesses  $2.42\text{ }\mu\text{m}$  or less, there was little or no change in the BRDF. As the water film thickness increased from  $2.4\text{ }\mu\text{m}$  to  $2.9\text{ }\mu\text{m}$ , note the large increase in the BRDF. This is attributed to an effect noted by Arnold (Ref. 12) as shattering or fracturing of the contaminant film surface. When this increase in scattering occurs, the illuminated spot on the superpolished mirror becomes very bright to the unaided eye, and the interior of the BRDF chamber becomes visually illuminated by the scattered light.

## 4.2 SPQCM DATA

### 4.2.1 Nitrogen on SPQCM

BRDF scans were made of nitrogen contaminant films on the 15 K SPQCM surface. Selected BRDF scans for nitrogen film thicknesses of  $0.25$ ,  $0.75$ , and  $5.02\text{ }\mu\text{m}$  are presented in Fig. 5. Not shown are BRDF scans for other film thicknesses up to  $8.25\text{ }\mu\text{m}$ . The cause of the small peak in the BRDF at  $20\text{ deg}$  is uncertain. It may be a characteristic of the measuring instrument. For the nitrogen contaminant films, the BRDF increased gradually with nitrogen contaminant film thickness over the range of angles and thicknesses studied. For nitrogen film thicknesses less than  $0.75\text{ }\mu\text{m}$ , the BRDF increased less than a factor of two from the pretest condition, and for film thickness of  $5\text{ }\mu\text{m}$ , the BRDF increase from the pretest condition was still less than a factor of four. Compared with the other gases used, the effect of the nitrogen film on the BRDF appears to be small.

Monitoring the scattered radiation, the scattering angle of  $5\text{ deg}$  showed a gradual increase in the BRDF as the film thickness increased with no sudden increase. There was a small periodicity that followed the specular interference fringe maxima. This is seen in Fig. 6, which presents the  $5\text{-deg}$  BRDF against the SPQCM output or difference frequency. The change in frequency shown in Fig. 6 (about  $65\text{ kHz}$ ) represents an approximate film thickness of  $2.5\text{ }\mu\text{m}$ . The frequency range shown was limited by the range of the counter in the model 1819 controller and not the SPQCM. An alternate counter, not tied to the data system but with a visual display, allowed the higher SPQCM frequencies to be read. The SPQCM frequency at the interference fringe maxima was manually written on the strip chart next to the interference fringe maxima. The SPQCM performed well for the nitrogen run, giving a frequency change of approximately  $260\text{ kHz}$  for the  $8.25\text{-}\mu\text{m}$ -thick contaminant film. These data are presented in Fig. 7. Note the change in slope, particularly beyond 20 interference fringe maxima. This slope change might be from different nitrogen density attributed to changing the contaminant film deposition rate. The first five micrometers of contaminant film were deposited at an approximate rate of  $0.05\text{ }\mu\text{m}/\text{min}$ , whereas the last three micrometers were deposited at an approximate rate of  $1.3\text{ }\mu\text{m}/\text{min}$ . A more likely cause of the line slope

change is nonlinearity of the SPQCM. Previous experience with QCMs indicates that the output frequency change with mass addition may deviate from linearity when frequencies much greater than 100 kHz are encountered. This nonlinearity is also described by Wallace (Ref. 13). The deviation of the upper portions of the curve (Fig. 7) may be caused by the QCM nonlinearity rather than a density change for nitrogen. A linear fit was made to the first sixteen fringe maxima, from which density of nitrogen was calculated to be 1.07 gm/cm<sup>3</sup> compared with 1.03 gm/cm<sup>3</sup> in Ref. 14.

#### 4.2.2 Oxygen on SPQCM

Oxygen was condensed on the 15 K SPQCM surface, and BRDF scans were made for contaminant thicknesses between 0.25 and 2.53  $\mu\text{m}$  (Fig. 8). The oxygen contaminant film had a major effect on the BRDF. The BRDF curves are essentially flat, showing the oxygen film to be a diffuse surface with reflectivity varying with the thickness. The minimum oxygen contaminant thickness measured, 0.25  $\mu\text{m}$ , caused order-of-magnitude changes in the BRDF at angles greater than 10 deg. Two runs were made on consecutive days. On the first run, oxygen contamination was started, then the SPQCM was warmed to 40 K to remove the oxygen. The precontamination BRDF scan was repeated, showed no change in the BRDF, and the oxygen contamination resumed. These are the results presented in Fig. 8a. After the run was completed, the chamber was warmed overnight and the SPQCM crystal was heated to 340 K to remove traces of contaminants. The next day, the chamber was recooled, and the oxygen deposit run was repeated (Fig. 8b). Both runs had essentially identical BRDF scans prior to contamination. However, the BRDF scans of the contaminant layers showed much higher BRDF values for the second run. In particular, the 0.25- $\mu\text{m}$  layer on the second run has nearly an order-of-magnitude greater BRDF scatter than the 0.25- $\mu\text{m}$  layer of the first run. Examination of the SPQCM frequency on the second run showed a 100-Hz frequency increase prior to the start of the gas addition. This indicates that a small amount of some contaminant was deposited prior to starting the oxygen addition. The source of the frequency increase is uncertain, whether it was condensed nitrogen or some other contaminant source. This indicates that the BRDF of oxygen may be dependent on the conditions present as the contaminant is condensed. Another difference between the two runs may have occurred during the first day's run. During this first run, after evaporating the initial oxygen, contaminant residue may have remained on the superpolished surface prior to the second addition of oxygen. However, this was not evident from the comparisons of the BRDF scans prior to the oxygen contamination.

In Figs. 8a and b, both BRDF runs have a dip in the BRDF at 30 deg for a film thickness near  $2.5\text{ }\mu\text{m}$ . This may be scattering interference reported by Smith and Templemeyer (Ref. 15).

The variation in the BRDF at a scatter angle of 6 deg (6-deg BRDF) and the variation of the specular beam intensity as the film thickness increases (as indicated by the SPQCM frequency change) is shown in Figs. 9a and b. The specular interference maxima are clearly evident. From Eq. (3), each maxima represents an increase in the film thickness of  $0.25\text{ }\mu\text{m}$ . The BRDF scatter also shows interference maxima and minima. These maxima and minima are phase-shifted from the specular pattern.

The variation of the SPQCM frequency with the film thickness is shown in Fig. 10. The solid line represents the linear least-squares fit to the data points. The slight scatter of the points from the straight line is attributed to the uncertainty of locating the interference maximum and reading the SPQCM frequency as the oxygen was being added. Using the slope of the linear fit and Eq. (11), the average density of the 15 K oxygen deposit was determined to be  $1.45\text{ gm/cm}^3$ , compared with  $1.43\text{ gm/cm}^3$  in Ref. 14.

The warmup of the SPQCM crystal at  $2.5\text{ K/min}$  is shown in Figs. 11a, b, and c. Using the estimated chamber pressure (approximately  $10\text{E}-7\text{ torr}$ ), the oxygen vapor pressure predicts that the oxygen would start evaporating from the SPQCM somewhere near 32 K. However, from the 6-deg BRDF scatter plot and the QCM frequency plot, the majority of the cryofilm evaporated from the SPQCM at a temperature near 40 K. This observation that the cryofilm evaporated at higher than predicted temperatures was typical of many of the warmups of other QCMs. A possible explanation is that during warmup, a temperature gradient exists across the QCM crystal pack. This gradient may be such that the sample crystal temperature was at a lower temperature than the crystal pack temperature sensor (located in the middle of the crystal pack). The specular beam intensity (Fig. 11b) also shows a disturbance at 40 K. The cause of this dip in the intensity of the reflected specular beam during the evaporation from the SPQCM is unexplained. SPQCM frequency changes at temperatures above 150 K are attributed to changes in the SPQCM base temperature when the helium refrigerator had been turned off and the system was rapidly warming to ambient. During one SPQCM evaluation run, this SPQCM was observed to have approximately 1,000-Hz drop in output frequency over a similar excursion of the base temperature.

#### 4.2.3 Carbon Dioxide on SPQCM

Selected BRDF scans are shown for two runs using carbon dioxide as the contaminant on 20 K and 15 K SPQCM surface (Fig. 12). The first run with carbon dioxide condensed on the 20 K surface did not show major changes until the cryofilm passed  $1.5\text{-}\mu\text{m}$  thickness. Then the BRDF increased rapidly. The second run with carbon dioxide on the 15 K SPQCM showed a large BRDF increase at  $1.0\text{-}\mu\text{m}$  film thickness. This appears to be a case of the contaminant film shattering. These BRDF profiles before shattering are not as flat as the

oxygen BRDF profiles. This shows that before shattering, the carbon dioxide films are less diffuse than the oxygen films. For the first run with the 20 K surface, Fig. 13 shows the increase in the 6-deg BRDF and the variation in specular intensity as the SPQCM frequency increases. In this figure, the onset of the large BRDF increase is easier to locate than in the BRDF profiles. From the 6-deg BRDF, the major scatter increase starts near maxima number 7, corresponding to a contaminant film thickness of  $1.75 \mu\text{m}$ . When this large increase in the scatter occurs, the fringe maxima and minima become more irregular for both the specular intensity and the 6-deg scatter. The 15 K case (not shown) was even worse with only four distinct, regular fringes. Note that shattering was not seen for the warmer temperatures with the superpolished mirror (40 to 50 K). It is uncertain whether the differences between the 20 K and the 15 K carbon dioxide runs are caused by the temperature differences or some other, unknown, cause.

The linearity between the SPQCM frequency and the film thickness is presented for the 20 K surface in Fig. 14. The lack of curvature of the data indicates the density of the carbon dioxide is not varying significantly with film thickness. The slope of the least-squares linear fit to these data (9,138-Hz/fringe maxima) gives an average density for the carbon dioxide film of  $1.38 \text{ gm/cm}_3$ .

On warming, the SPQCM oscillator quit and did not recover until most of the contaminant film had evaporated. It has been noticed with both this SPQCM and other QCMs that they often cease oscillating while the contaminant film is evaporating from the crystal.

#### 4.2.4 Water on SPQCM

Five runs were made while attempting to inject water without an air component. To aid in evaluating the water injection, a second conventional QCM was mounted in the injection plume and operated with a crystal temperature cold enough to condense water, yet too warm to condense oxygen and nitrogen. The run with a minimal air component is presented. Figure 15 shows the BRDF for water condensed on the 27 K SPQCM crystal surface. Note the increase in the BRDF that occurred after  $0.49\text{-}\mu\text{m}$  thickness was obtained. With approximately  $1.5\text{-}\mu\text{m}$  water film thickness, the BRDF increased three orders of magnitude. For comparison, the 40 K case (Fig. 4) showed that the rapid increase happened at a film thickness between  $2.4$  and  $2.9 \mu\text{m}$ . This shattering of the surface was typical of the condensed water (ice) films encountered. Fracture of the condensed film was observed on all runs where water was deposited. The only variations were the surface temperature and the thickness where the fracture occurred. When the condensed film fractured, the SPQCM would nearly always quit, usually at a relatively low frequency, and the BRDF increased two or three orders of magnitude (Fig. 16). The density of the water was determined for three of the water runs using the first 2 or 3 interference fringe maxima and minima available before the film surface fractured. The following three densities were obtained for water films condensed on a 23

to 27 K surface: 0.981, 0.946, and 0.902 gm/cm<sup>3</sup>. From these values the average water density is 0.943 gm/cm<sup>3</sup>. The density of ice at 0°C is 0.917 (Ref. 14).

The SPQCM was warmed at a rate of 2.5 K/min until the water evaporated. As evidenced by the decrease in the 6-deg BRDF (Fig. 17), the water evaporated about 180 K. This is about 20 K warmer than predicted from the 10E-7 torr chamber pressure.

#### 4.2.5 Layers, Nitrogen then Carbon Dioxide on SPQCM

A 2.5- $\mu$ m-thick contaminant film of nitrogen was deposited on the 16 K SPQCM surface, then a 2.5- $\mu$ m-thick layer of carbon dioxide was applied over the nitrogen. The effect on the BRDF is shown in Fig. 18. With the exception of the dips in the BRDF profiles, the BRDF values appear to be similar to the case of carbon dioxide alone. The nitrogen made only minor changes in the BRDF, while the carbon dioxide made order-of-magnitude changes in the BRDF as the carbon dioxide films were deposited on top of the nitrogen. The magnitudes of the BRDF changes with thickness appear to lie between the effects measured with the previously discussed 15 and 20 K carbon dioxide-only runs (Fig. 12). The dips occurring at 20-deg scatter angle may be similar to those observed earlier (Fig. 8). The 6-deg BRDF scatter increase with the SPQCM frequency (Fig. 19) shows essentially the same thing. From the lack in definition of the scatter fringes and the sharp rise in the BRDF as the carbon dioxide was added, one would conclude that the film surface had fractured. There is no obvious reason for the step in the 6-deg BRDF curve that occurred at about 120 kHz.

Figure 20 shows the comparison of the SPQCM frequency with the interference fringe maxima. There are two distinct slopes present corresponding to the two layers of nitrogen and carbon dioxide. The density for nitrogen, 1.08 gm/cm<sup>3</sup>, was taken from the lower portion of this curve. This agrees with the 1.07 gm/cm<sup>3</sup> obtained for the first portion of the nitrogen-only contaminant film obtained at the lower deposition rate (Fig. 7). The carbon dioxide portion of Fig. 20 gave a density for carbon dioxide of 1.46 gm/cm<sup>3</sup>, which is near the 1.38 gm/cm<sup>3</sup> value reported for carbon dioxide earlier (Fig. 14).

The warming of the SPQCM (2.5 K/min) is shown in Fig. 21. There are scattering peaks in the vicinity of 38 K and 110 K which are noticeably higher temperatures than the 25 K nitrogen evaporation temperature and the 81 K carbon dioxide evaporation temperature. The causes of these scattering peaks are uncertain. Near 165 K, the 6-deg BRDF approaches the uncontaminated level. The water evaporation temperature is about 158 K, which indicates that some water was present in the contamination film in spite of precautions.

#### 4.2.6 Layers, Carbon Dioxide then Nitrogen on SPQCM

A film of carbon dioxide contaminant, 1.5- $\mu$ m thick, was deposited on the 15 K SPQCM surface, then a 1.5- $\mu$ m film of nitrogen was condensed on top of the carbon dioxide. The



BRDF measurements of these films are shown in Figs. 22 and 23. The BRDF of the carbon dioxide layers shows the signs of shattering while the nitrogen has only small effects on the BRDF. It appears to be just the reverse of the previously discussed carbon dioxide layer over a nitrogen layer with no surprises.

The 6-deg BRDF during the SPQCM warmup is shown in Fig. 24 for a similar contamination run. The warmup shown had the same total thickness as used for Fig. 21. The warming rate was 1 K/min for temperatures less than 45 K. In this case, there are scattering peaks in the vicinity of 34 K, 100 K, and 150 K with large decreases in the 6-deg BRDF as the carbon dioxide and the water evaporated. These scatter peaks occur at a 5 to 10 K lower temperature than the carbon dioxide over nitrogen case (Fig. 21), but they are still above the predicted evaporation temperature.

#### **4.2.7 Mixed Gas, N<sub>2</sub>, O<sub>2</sub> and CO<sub>2</sub> on SPQCM**

A mixed gas sample consisting of equal parts by pressure of nitrogen, oxygen, and carbon dioxide was used to contaminate the SPQCM at 16 K. The BRDF for selected contaminant thicknesses up to 3.5  $\mu\text{m}$  is shown in Fig. 25, and the 6-deg BRDF is shown in Fig. 26. Note that for this case there was no fracture of the contaminant film typical of carbon dioxide, no strong diffuse scattering seen with oxygen, and the 6-deg BRDF only increases by about a factor of two. This is in sharp contrast with the cases where oxygen or carbon dioxide existed in separate layers. The density obtained for this mixture at 16 K was 1.34 gm/cm<sup>3</sup>. For comparison, the average of the measured densities of the individual gases is 1.30 gm/cm<sup>3</sup>.

### **4.3 DATA UNCERTAINTY**

#### **4.3.1 Superpolished Mirror Surface Temperature**

The silicon-diode temperature sensor for the superpolished mirror was mounted on the rear surface of the mirror. Because of the limited surface available for attachment, the temperature sensor was attached next to the mirror heater, which was also attached to the rear surface. The temperature sensor had an accuracy of better than 2 K, but this was not the major limitation in the measurement of the temperature of the mirror front surface. Temperature gradients were present that reduced the accuracy of the measurement. One potential source of temperature gradient came from the mirror mount. The mount consisted of a tapered ring around the front edge of the mirror with an aluminum slug in the rear, behind the heater. The mirror was clamped between the metal ring and the aluminum slug with the entire assembly mounted in the helium-cooled block. Conductive heat-transfer paths for the mirror were through the front ring to the helium-cooled block and through the heater to the block. The temperature gradient between the front surface and the temperature sensor is difficult to determine. It is estimated that as much as 5 K uncertainty may exist during a rapid cooling and 10 K uncertainty when heat is applied with the mirror heater. The uncertainty is all bias error (in contrast to a random error).

### 4.3.2 SPQCM Crystal Surface Temperature

Temperature differences can exist between the sensing crystal surface temperature and the SPQCM temperature sensor. Both quartz crystals, the silicon-diode temperature sensor, and the heater are mounted together in the crystal pack (Fig. 2). The front sensing crystal makes contact with its copper mounting plate around the outer edge. This mount produces a poor thermal path. The silicon-diode temperature sensor is mounted in a copper plate in the center of the crystal pack, and the heater is mounted in a copper plate at the rear of the crystal pack. Glassford (Ref. 4) analyzed a QCM of similar design in the vicinity of 100 K that was assumed to be in thermal equilibrium. Glassford evaluated the heat loss from the crystal by radiation to the cold chamber wall and by evaporation of the contaminant. He estimated a 0.1 K temperature gradient existed between the temperature sensor and crystal surface. For the BRDF chamber, the situation was more complex. The BRDF chamber had a helium-cooled cryopanel at approximately 15 K, a nitrogen-cooled liner at approximately 77 K, and the BRDF arm assembly and mounting plate at approximately 300 K. The SPQCM sense crystal, near 15 K, exchanged radiation with these surfaces. During steady state, the temperature difference should still be less than 1 K. When the SPQCM is being cooled or heated at rates greater than 1 K/min, larger temperature differences between the sensor and crystal surface could exist. The silicon-diode temperature sensor is rated by the manufacturer to have less than 1.5 K error for the 10 to 100 K range, the main region of interest. Calibration of the QCM research model 1819 QCM controller was adjusted to be within 0.8 K. For equilibrium, the root-sum-square of the error contributions gave an estimated uncertainty for the SPQCM surface temperature of 2 K, all of which is a bias error.

### 4.3.3 SPQCM Mass per Area

For a QCM, the relation between mass deposited on the sense crystal per area and the measured frequency change is given by Eq. (1) and Eq. (2). The fundamental frequency of the SPQCM crystal was measured to be 10.960 MHz with an uncertainty of 2 KHz, or 0.2 percent. The crystal constants are also known to this accuracy (Ref. 3). The temperature variation of these crystal constants between 300 K and 10 K is less than 0.02 percent (Ref. 3), which is negligible. The variation of the proportionality constant,  $C$ , with mass added (i.e., QCM frequency linearity with mass added) is given (Ref. 13) as less than 2 percent for frequency changes less than 100 kHz. An estimate of the SPQCM nonlinearity above 100 kHz can be made using Fig. 7. Assuming the nitrogen contaminant deposited at a constant density and the change in slope is due only to the nonlinearity of the SPQCM, a nonlinearity estimate of 25 percent for frequency can be obtained. The measurement of the SPQCM output frequency,  $df$ , was limited by the noise on the signal going into the frequency counters. This SPQCM (in contrast to some QCMs used) had a strong signal with minimal noise. In addition, filtered preamplifiers were used along with an oscilloscope to monitor the amplitude and

noise and optimize the signal for the frequency counter input. During these measurements, it is estimated that the frequency count error was less than 2 Hz for frequencies less than 50 kHz and less than 10 Hz for frequencies between 50 and 100 kHz. This error grew as the output frequency of the SPQCM increased above 100 kHz. The primary change was due to the decreasing signal amplitude (hence signal to noise) as the crystal contaminant load was increased. At output frequencies above 150 kHz, the error could be as high as 500 Hz. Thus, for the SPQCM counter configuration used, the SPQCM output frequency counting error was less than 0.1 percent below 100 kHz. The SPQCM output frequency varied with the temperature of its base. An 800-Hz shift was observed when this SPQCM cooled from 300 K to 16 K during the initial SPQCM checkout. This base temperature sensitivity requires the SPQCM base to be at a stable temperature when small frequency changes are to be observed. For most of the contaminant runs, this stability of base temperature was maintained until the helium cooling was turned off.

The total uncertainty of the mass per area determination varied with the mass load on the crystal and the stability of the SPQCM base temperature. For a constant base temperature, the total uncertainty of  $dm/A$  was limited by the SPQCM linearity to 2 percent for frequencies less than 100 kHz and rising to 25 percent at 260 kHz. Changes in the base temperature cause an additional frequency shift of approximately 3 Hz/K in addition to the nonlinearity. This estimated uncertainty is all bias error.

#### 4.3.4 Thickness Measurement and Density

The relation to obtain the film thickness from the interference fringe maxima was given by Eq. (3). The dominating quantities near normal laser beam incidence are the film refractive index and the location of the interference fringe maxima. The refractive index has a reported error of 2 percent (Ref. 5). By examining the interference fringe cycles of the specular beam intensity recorded on the strip chart recorder, it was estimated that an interference fringe maxima could be located to within 5 percent of a cycle. From Eq. (3), one interference fringe cycle was calculated to be approximately  $0.25 \mu\text{m}$ , giving an estimated uncertainty of  $0.013 \mu\text{m}$  in locating the interference fringe maximum. Since the fringe maximum is a periodic function, the relative error in the thickness from locating the maximum will decrease inversely proportional to the number of maxima used. For example, using 2 fringe maxima would give approximately 2.5-percent error from locating the fringe maximum while using 10 fringe maxima reduces this source of error to approximately 0.5 percent. Combining the two errors from refractive index and fringe maximum location, and using the root-sum-squares gives an estimate of the total uncertainty for the thickness. These bias errors are 3 percent for water (2 fringes) and 2 percent for all other gases (10 fringes).

The density was calculated using Eq. (11). The density determination is composed of two components —  $dm/A$  from the SPQCM, and the thickness from the specular beam monitor. For the conditions of the density determination,  $dm/A$  had an uncertainty of 2 percent. The estimated combined uncertainty for the density determination is 4 percent for water (2 fringes) and 3 percent for all other gases (10 fringes).

#### 4.3.5 BRDF Determination

The BRDF was determined using Eq. (10). This method required a detector voltage measurement with a known diffuser in the sample position. Then measurements were made of detector voltage at different angles with the superpolished mirror or SPQCM in the sample position. The errors in this technique were discussed by Young (Ref. 1).

In general, the major source of error in BRDF measurements is caused by stray light. Some of the causes of the stray light in the BRDF chamber and the steps taken to reduce the stray light effects were discussed in Section 2.2. The error contribution from stray light sources is difficult to quantify. To see if significant stray light sources remained, comparisons were made between measurements made on the SPQCM prior to installation in the BRDF chamber using a different measuring apparatus, and measurements made in the BRDF chamber after installing the mask on the SPQCM and redesigning the specular beam dump assembly. The comparison did not indicate any major stray light problems. The differences between the BRDF values measured varied with angular position. At 10 deg, the BRDF after installation in the chamber was approximately 30 percent lower than the preinstallation value; at 20 deg, the values agreed; and at 30 deg, the values were 20-percent higher.

Detector linearity for a similar detector and amplifier system was investigated by Young (Ref. 1). The conclusion was that the maximum deviation from linearity was less than 8 percent.

The diffuser reference method for determining the BRDF of the mirror requires knowledge of the reflectance of the reference diffuser near normal. This reflectance was listed as 0.98 at  $0.6328\ \mu\text{m}$ . Visually inspecting the sample, the reflectance should not be degraded by more than 5 percent, which is a small uncertainty compared with other sources of error.

The laser power drift was monitored by measuring the laser power output before each BRDF scan and comparing it to the laser power when the reference diffuser was measured. After time was allowed for the laser to reach operating temperature, the power did not change by more than 1 percent.

The scattering angle was measured from specular, which required the detector arm position to be referenced to the center of specular reflected laser beam. This was accomplished by

closing the detector shutter and rotating the detector arm until the specular beam was centered on a small bull's-eye marked on the shutter. The bull's-eye location matched the center of the detector assembly entrance aperture when the shutter was closed. That position was designated as the zero scatter angle. An estimated upper limit of the uncertainty for determining this position is 0.3 deg. For large angles, this had an insignificant effect compared with other sources of error. However, with a low scatter mirror like the SSG superpolished mirror, the BRDF changes rapidly with angle as the specular position is approached. For example, moving from 5.0 to 4.7 deg, the BRDF increased approximately 10 percent, but going from 2.0 to 1.7 deg the BRDF increased approximately 80 percent. These differences were observed comparing the pretest and installed BRDF values for the SPQCM. The installed BRDF values at 2.0 deg were 30 to 50 percent lower than the measurement taken of the SPQCM prior to installation.

From the comparisons between different BRDF measurements of the SPQCM and the effects of detector arm positioning on the BRDF of a superpolished mirror, the total uncertainty of the BRDF of a superpolished surface is estimated to be less than 80 percent for angles less than 3 deg, 30 percent for angles between 3 and 10 deg, 15 percent for angles between 10 and 20 deg, and 30 percent for angles greater than about 25 deg. All of this uncertainty is a bias error.

## 5.0 CONCLUDING REMARKS

Experiments have been performed under vacuum to measure the degradation of the 0.6328- $\mu\text{m}$  bidirectional reflectance distribution function (BRDF) of a superpolished mirror and a SPQCM with condensed contaminant films. The contaminant films studied were nitrogen, oxygen, carbon dioxide, water vapor, layers with nitrogen over carbon dioxide and carbon dioxide over nitrogen, and a mixed gas of equal parts nitrogen, oxygen, and carbon dioxide. In addition, the density of many of the films on the SPQCM was measured and presented.

The following comments can be made about the contamination studies:

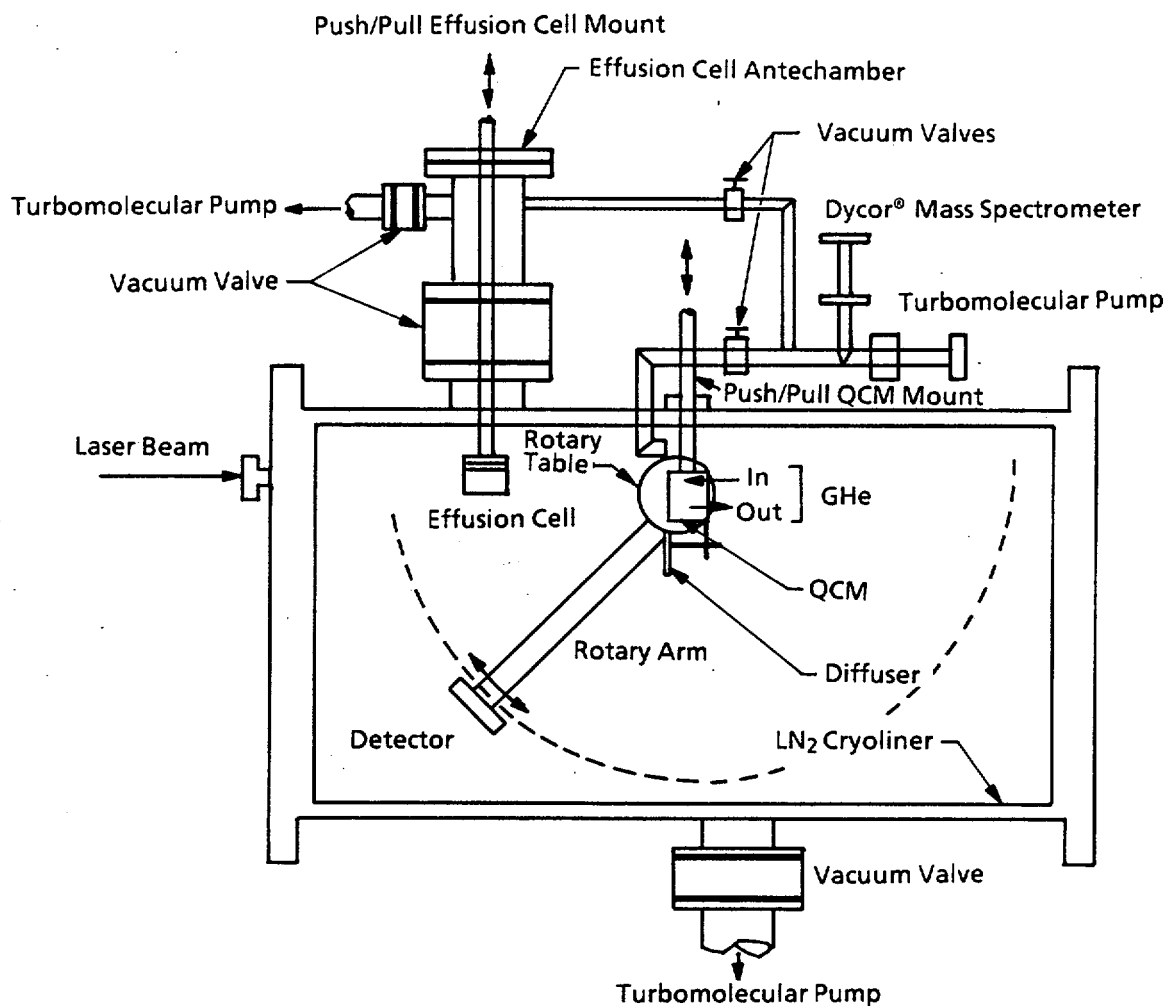
1. The SPQCM provided an excellent technique for characterizing changes in mirror BRDF with contaminant film thickness, even for films as thin as a few angstroms.
2. Nitrogen films had minimal effects on the BRDF for the temperature (15 K) and thicknesses (up to 8.25  $\mu\text{m}$ ) studied.

3. Oxygen on the 15 K surface had the most effect on the BRDF. A film as thin as 0.25  $\mu\text{m}$  acted like a diffuse surface with a flat BRDF profile and increased the BRDF two orders of magnitude.
4. Carbon dioxide increased the BRDF. At 15 to 20 K, it was observed to fracture with a 1.5- $\mu\text{m}$ -thick film, increasing its BRDF orders of magnitude. At 40 to 50 K, no fracture was observed, and the BRDF change was small.
5. Water contaminant films were observed to fracture at both 25 and 40 K for film thicknesses varying between 0.5 and 1.0  $\mu\text{m}$ . After shatter, water films had the highest BRDF values observed.
6. Layered nitrogen and carbon dioxide films at 15 K behaved much like the carbon dioxide component alone.
7. Mixed nitrogen, oxygen, and carbon dioxide on a 16 K surface was not observed to shatter and had little effect on the BRDF (less than a factor of two) for thicknesses up to 3.5  $\mu\text{m}$ . This result is contrary to what one might expect after looking at the results obtained earlier with individual layers of oxygen and carbon dioxide.
8. The mixed gas results need further study to better understand what prevents the oxygen and carbon dioxide from causing increased scatter.
9. The SPQCM provided an excellent technique for determining film density. The mass density was determined from the SPQCM, and the film thickness was determined from thin-film interference on the same surface.

## REFERENCES

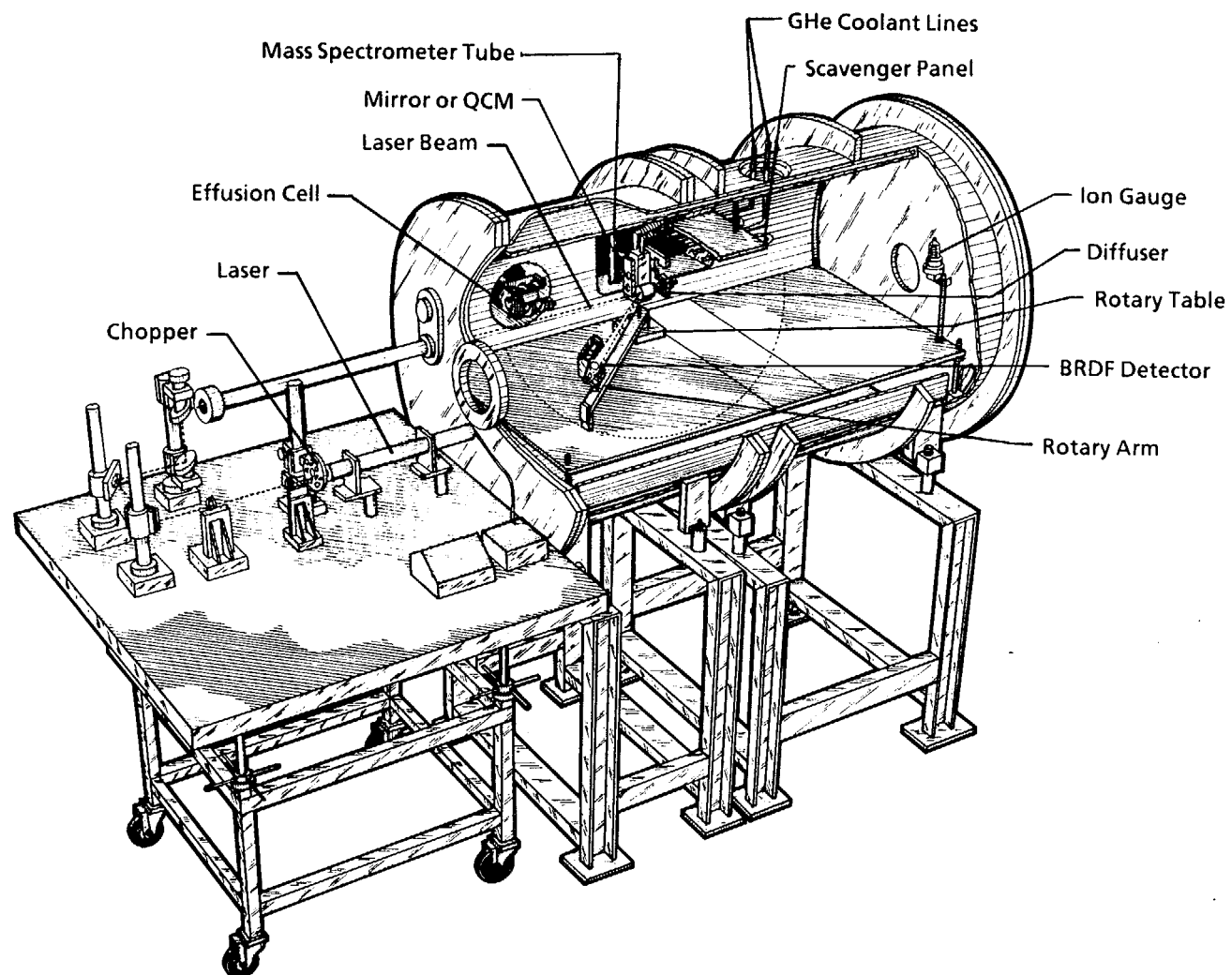
1. Young, R. P., Sr. "Metal Optics Scatter Measurements." SPIE Proceedings, Vol. 65. Design, Manufacture and Application of Metal Optics. August 19-20, 1975. San Diego, California (ISBN 0-89252-077-9), pp. 57-62.
2. Grum, F. and Luckey, G. W. "Optical Sphere Paint and a Working Standard of Reflectance." *Applied Optics*, Vol. 7, November 1968, pp. 2289-94.
3. Operation Manual for Quartz Crystal Microbalance QCM Sensor Mark 16. QCM Research, Laguna Beach, California.

4. Glassford, A. P. M. "Analysis of the Accuracy of a Commercial Quartz Crystal Microbalance." AIAA Paper No. 76-438, 11th Thermophysics Conference, July 14-16, 1976.
5. Wood, B. E., and Roux, J. A. "Infrared Optical Properties of Thin H<sub>2</sub>O, NH<sub>3</sub>, and CO<sub>2</sub> Cryofilms." *Journal of the Optical Society of America*, Vol. 72, No. 6, June 1982, pp. 720-28.
6. Nicodemus, F. E. "Directional Reflectance and Emissivity of an Opaque Surface." *Applied Optics*, Vol. 4, No. 7, July 1965, pp. 767-73.
7. Nicodemus, F. E. "Reflectance Nomenclature and Directional Reflectance and Emissivity." *Applied Optics*, Vol. 9, No. 6, June 1970, pp. 1474-75.
8. Nicodemus, F. E., et al. "Geometrical Considerations and Nomenclature for Reflectance." NBS Monograph 160, October 1977.
9. Williams, W. D., Bryson, R. J., Bertrand, W. T., and Jones, J. H. "Space Chambers Contamination Diagnostics and Analysis." AEDC-TR-90-18 (AD-A230248), December 1990, pp. 53-55.
10. Young, R. P. and Wood, B. E. "Bidirectional Reflectance Distribution (BRDF) of NASA Shuttle Tiles." AEDC-TSR-91-V1 (AD-A235115), April 1991.
11. Roux, J. A., et al., "Infrared Optical Properties of Thin CO, NO, CH<sub>4</sub>, HCl, N<sub>2</sub>O, O<sub>2</sub>, N<sub>2</sub>, Ar, and Air Cryofilms." AIAA Progress Series, Spacecraft Contamination: Sources and Prevention, eds. J. A. Roux and T. D. McCay, 1984, pp. 139-161.
12. Arnold, F. "Degradation of Low-Scatter Metal Mirrors by Cryodeposit Contamination." AEDC-TR-75-128 (AD-B007022L), October 1975.
13. Wallace, D. A. and Wallace, S. A. "Realistic Performance Specifications for Flight Quartz Crystal Microbalance Instruments for Contamination Measurement on Spacecraft." AIAA Paper No. 88-2727, Thermophysics, Plasmadynamics and Lasers Conference, San Antonio, Texas, 1988.
14. Weast, Robert C. Ed. *CRC Handbook of Chemistry and Physics*. Chemical Rubber Publishing Co., Cleveland, 1989 (1970 Edition).
15. Smith, A. M., Templemeyer, P. R., Muller, P. R., and Wood, B. E. "Angular Distribution of Visible and Near IR Radiation Reflected from CO<sub>2</sub> Cryodeposit." *AIAA Journal*, Vol. 7, No. 12, December 1969, pp. 2274-2280.



**a. Plan view of BRDF chamber**  
**Figure 1. BRDF Test Chamber.**





b. Three-dimensional view of chamber  
Figure 1. Concluded.

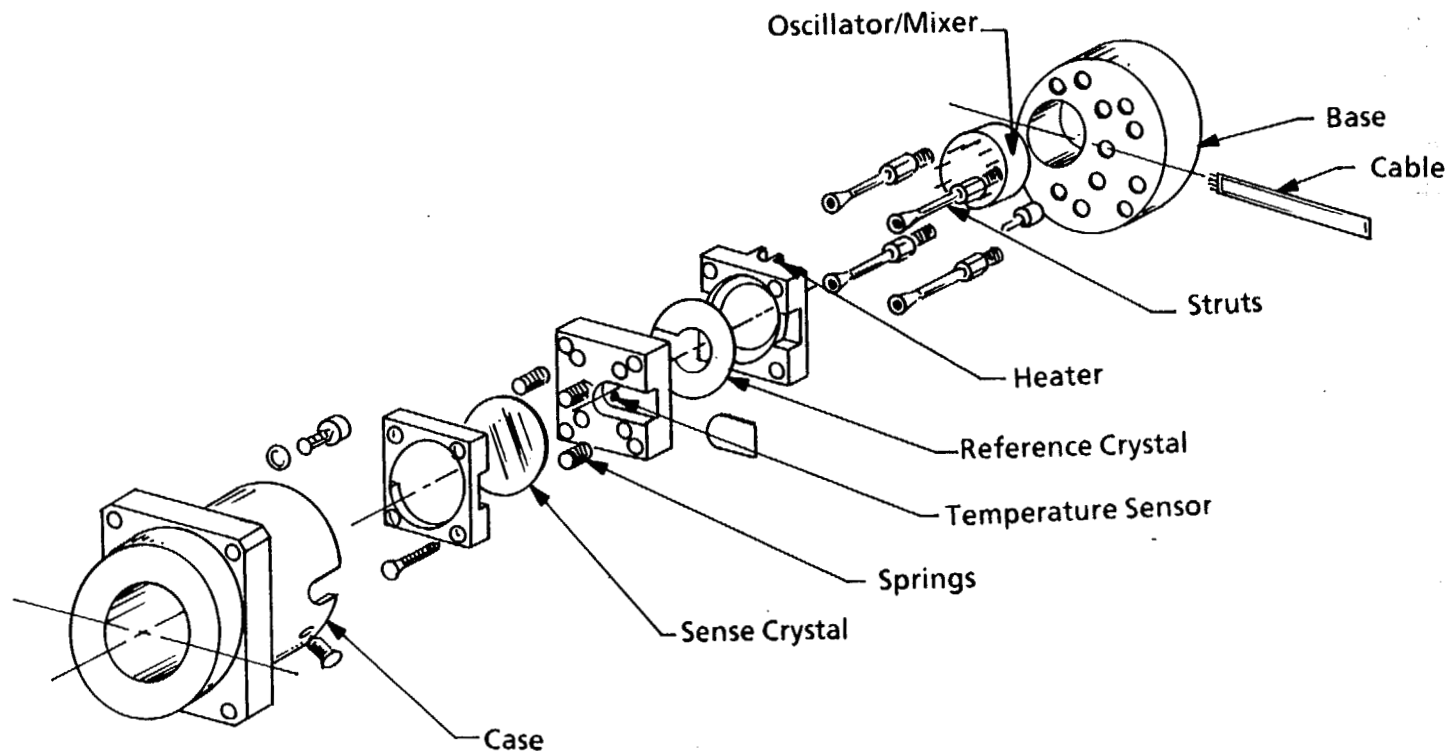


Figure 2. Exploded view of the Mark 16.

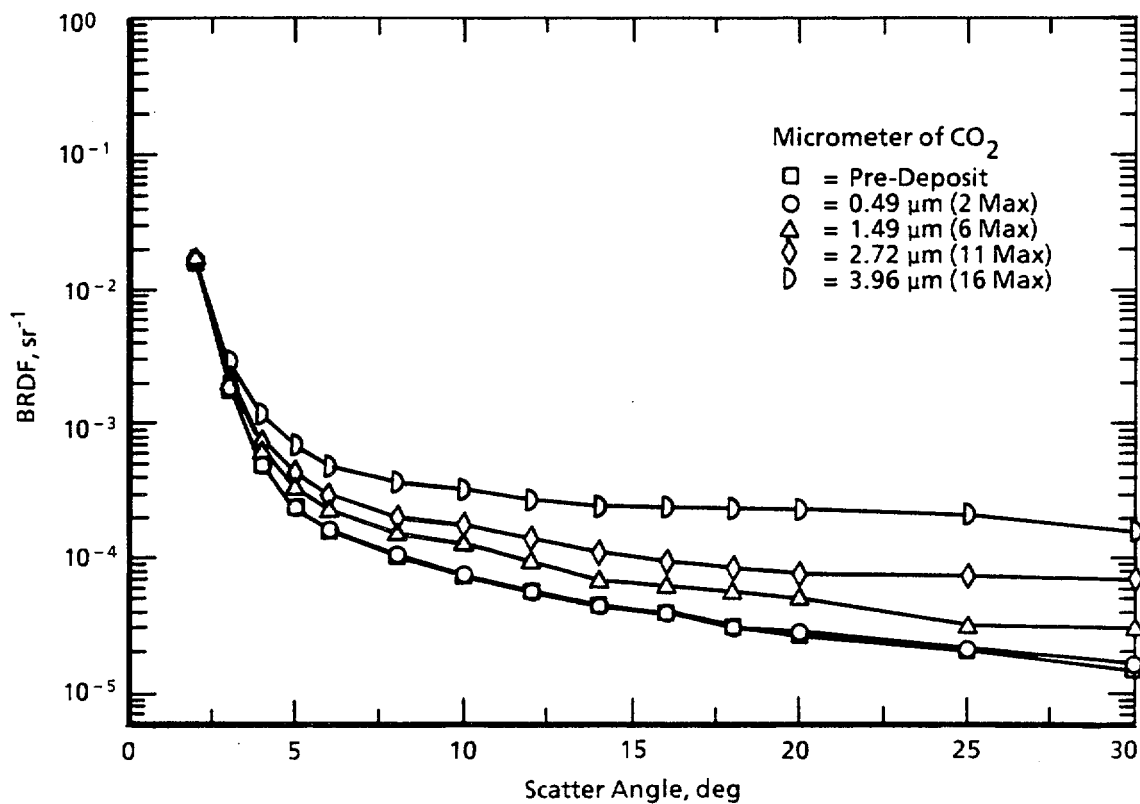


Figure 3. SSG superpolished mirror degradation at selected CO<sub>2</sub> film thickness; 40 K surface, 0.6328 μm.

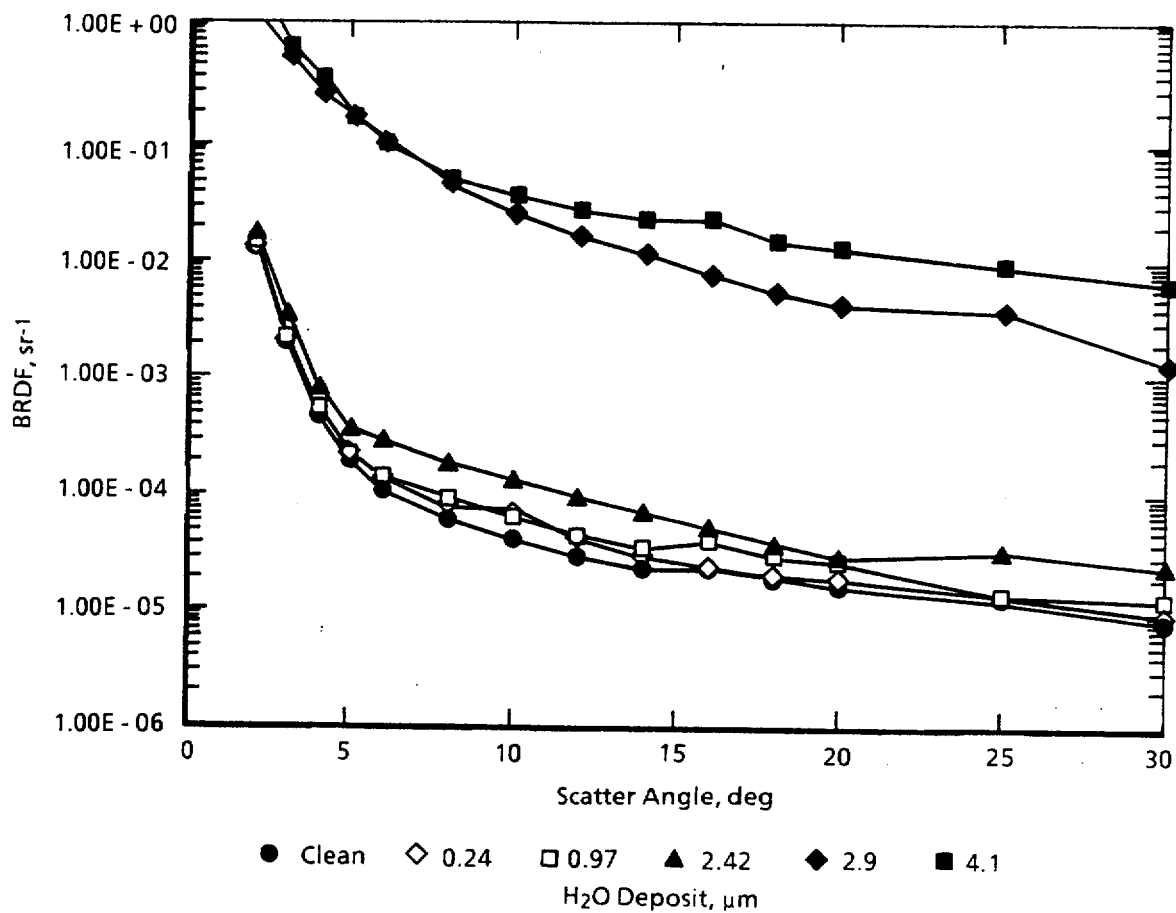


Figure 4. SSG superpolished mirror degradation at selected H<sub>2</sub>O film thickness; 40 K surface, 0.6328 μm.

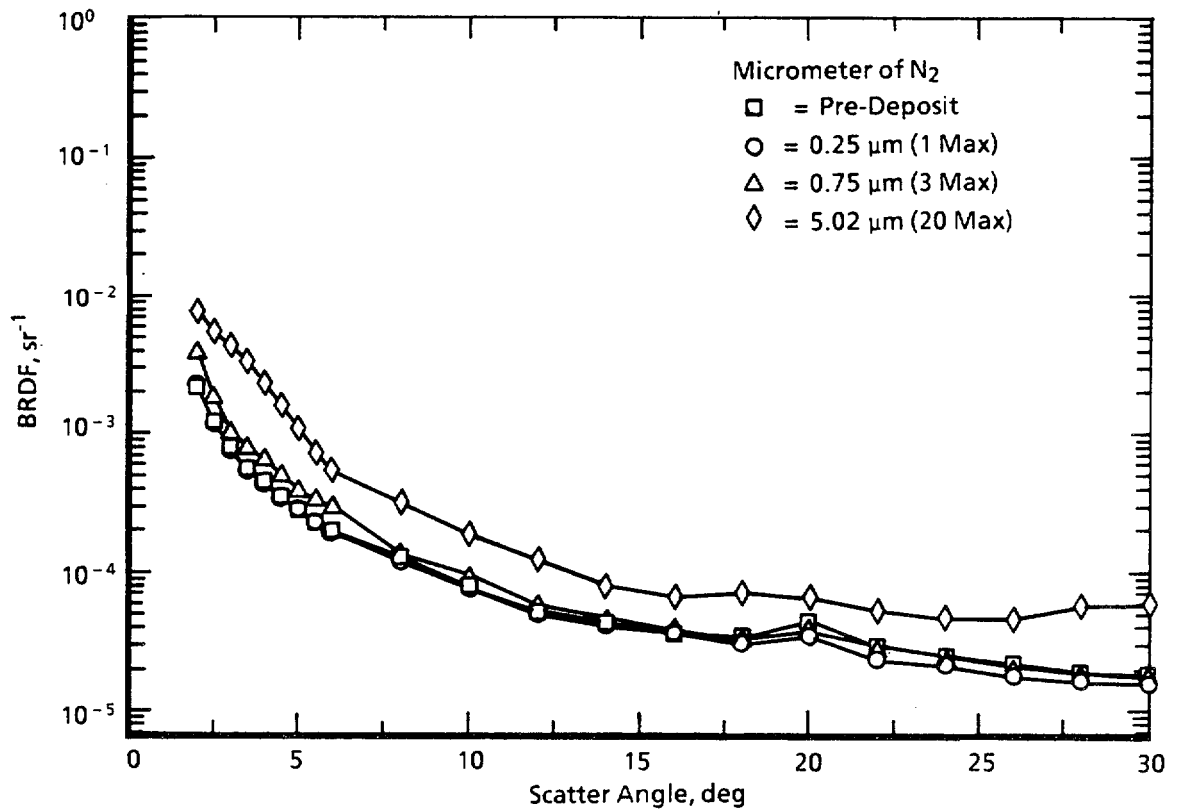
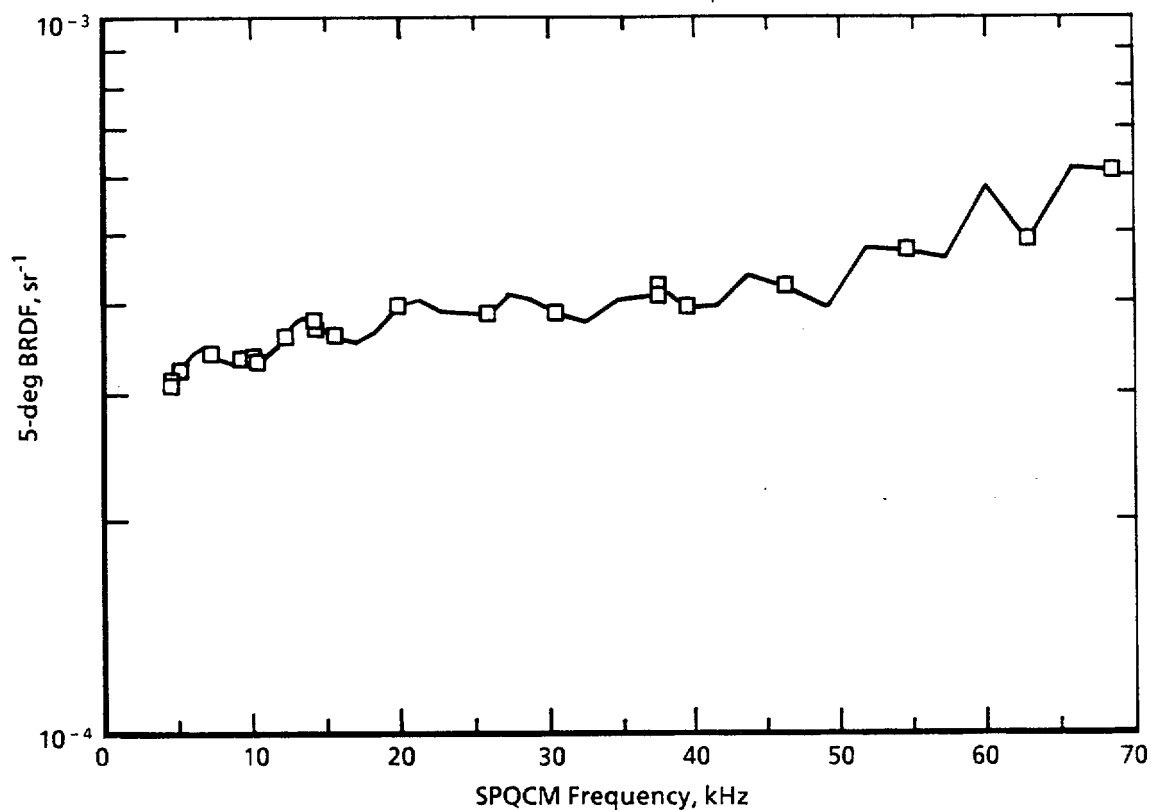
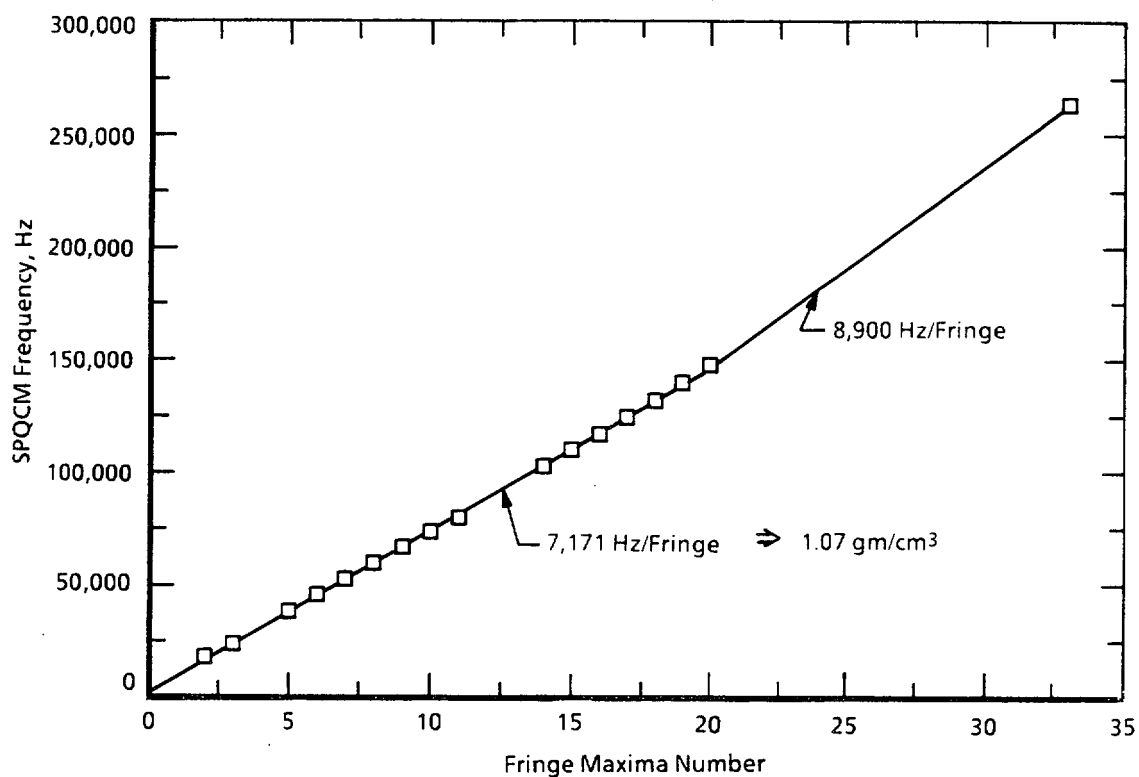


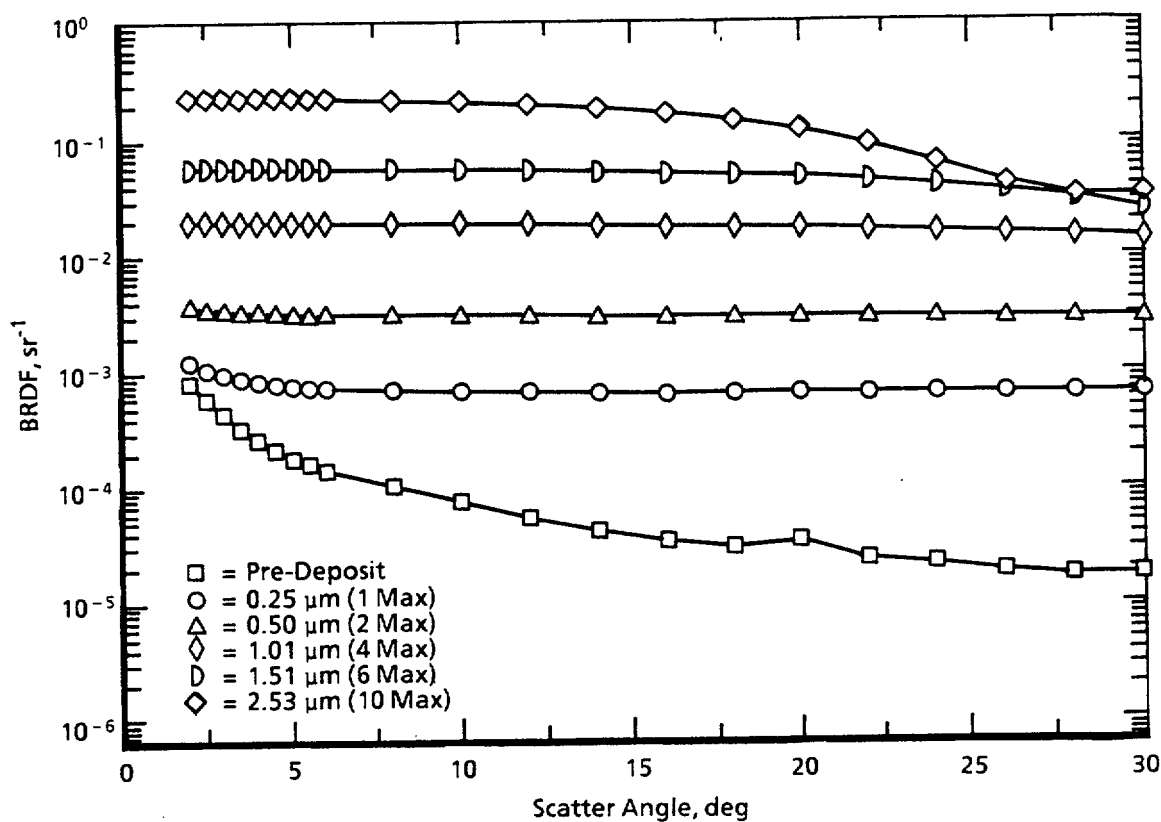
Figure 5. SPQCM degradation at selected  $\text{N}_2$  film thickness; 15 K surface, 0.6328  $\mu\text{m}$ .



**Figure 6. SPQCM 5-deg BRDF change with N<sub>2</sub> contamination; 15 K surface, 0.6328  $\mu$ m.**



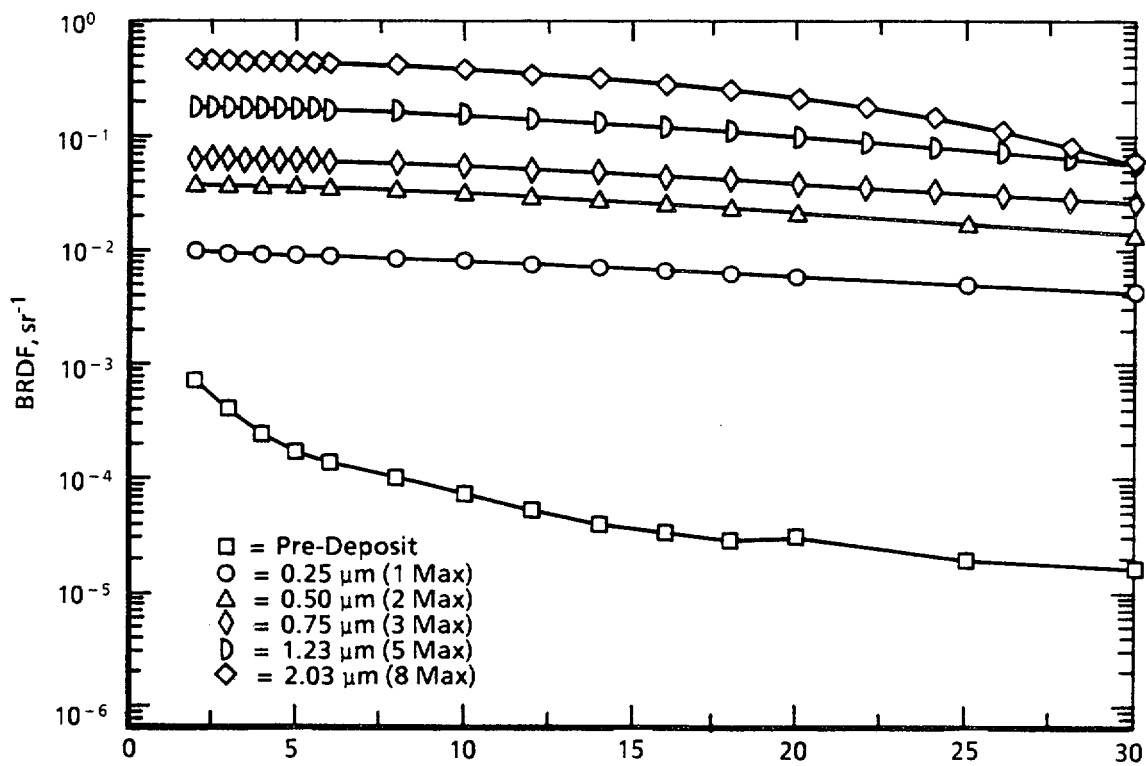
**Figure 7. Linearity of SPQCM frequency with nitrogen film thickness.**



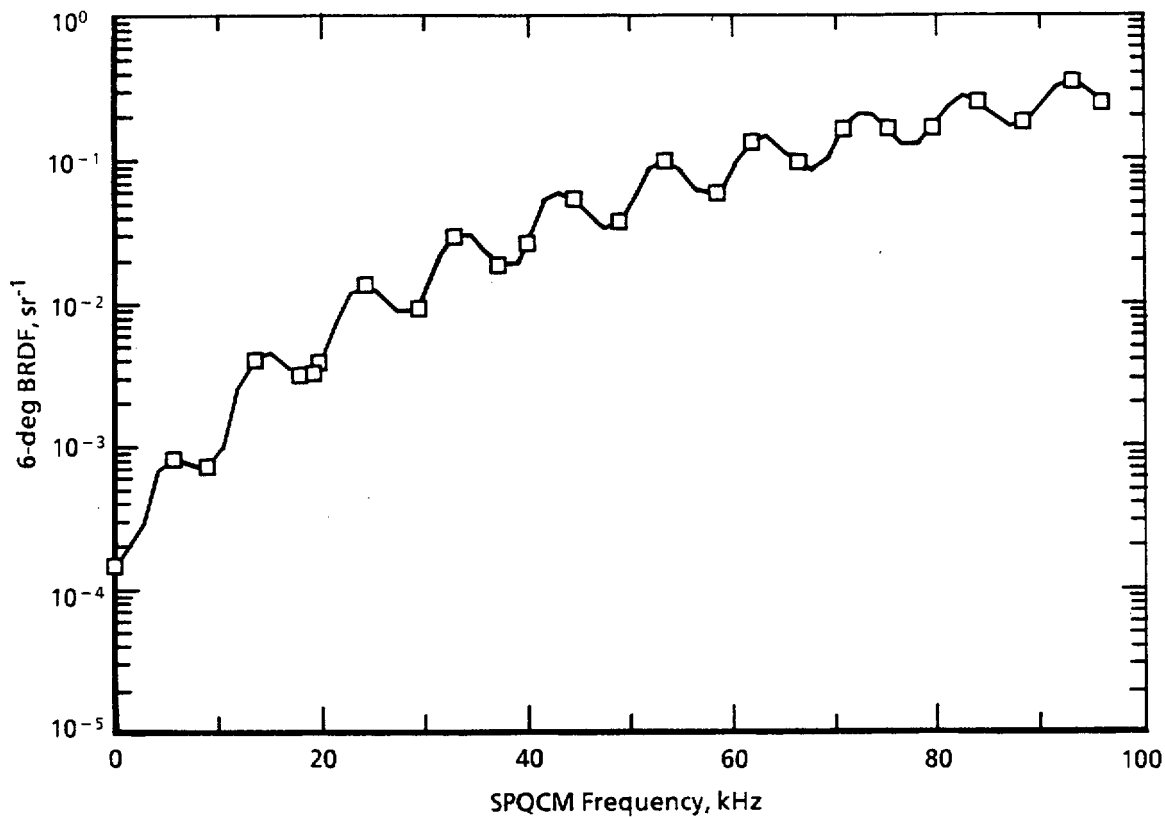
a. First  $\text{O}_2$  run

Figure 8. SPQCM degradation at selected  $\text{O}_2$  film thickness; 25 K surface, 0.6328  $\mu\text{m}$ .



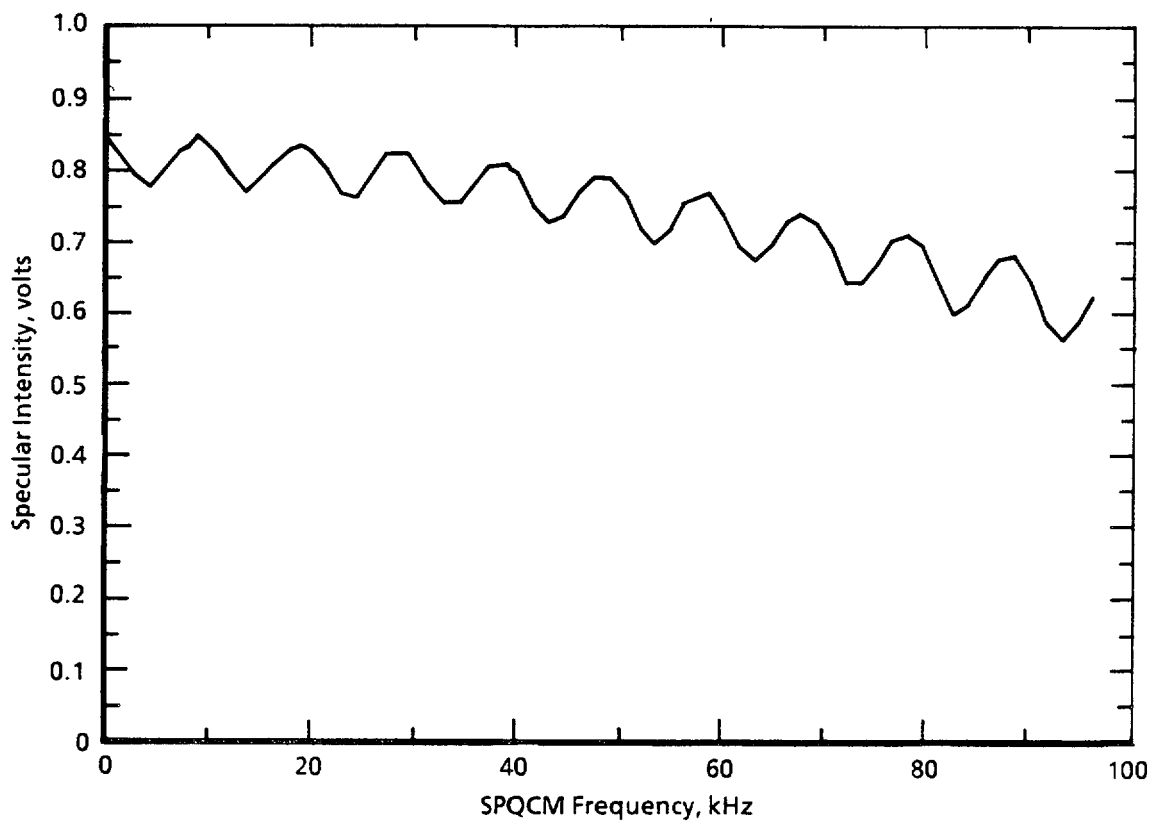


b. Repeat O<sub>2</sub> run  
Figure 8. Concluded.



a. Effect of O<sub>2</sub> on 6-deg BRDF

Figure 9. SPQCM with O<sub>2</sub> contamination; 15 K surface, 0.6328  $\mu\text{m}$ .



**b. Effect of O<sub>2</sub> contamination on specular intensity**  
**Figure 9. Concluded.**

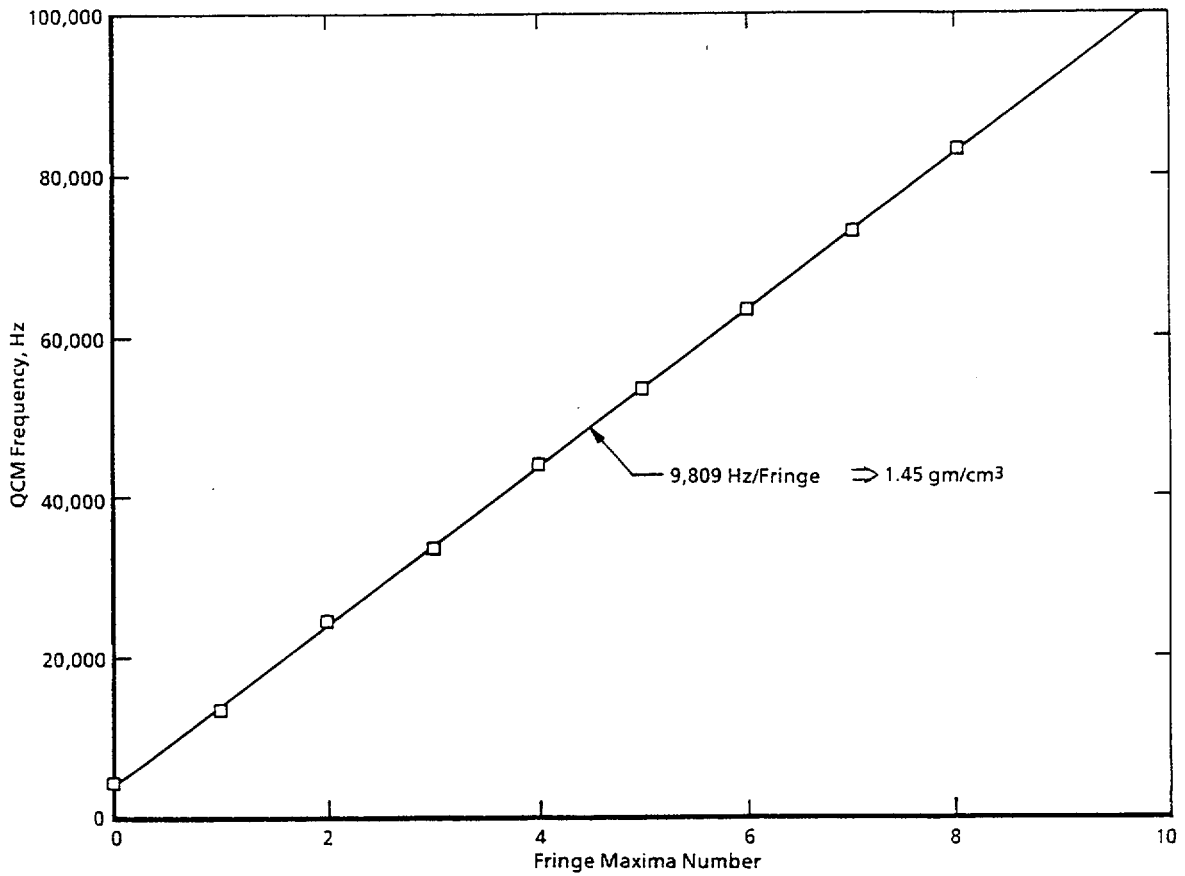
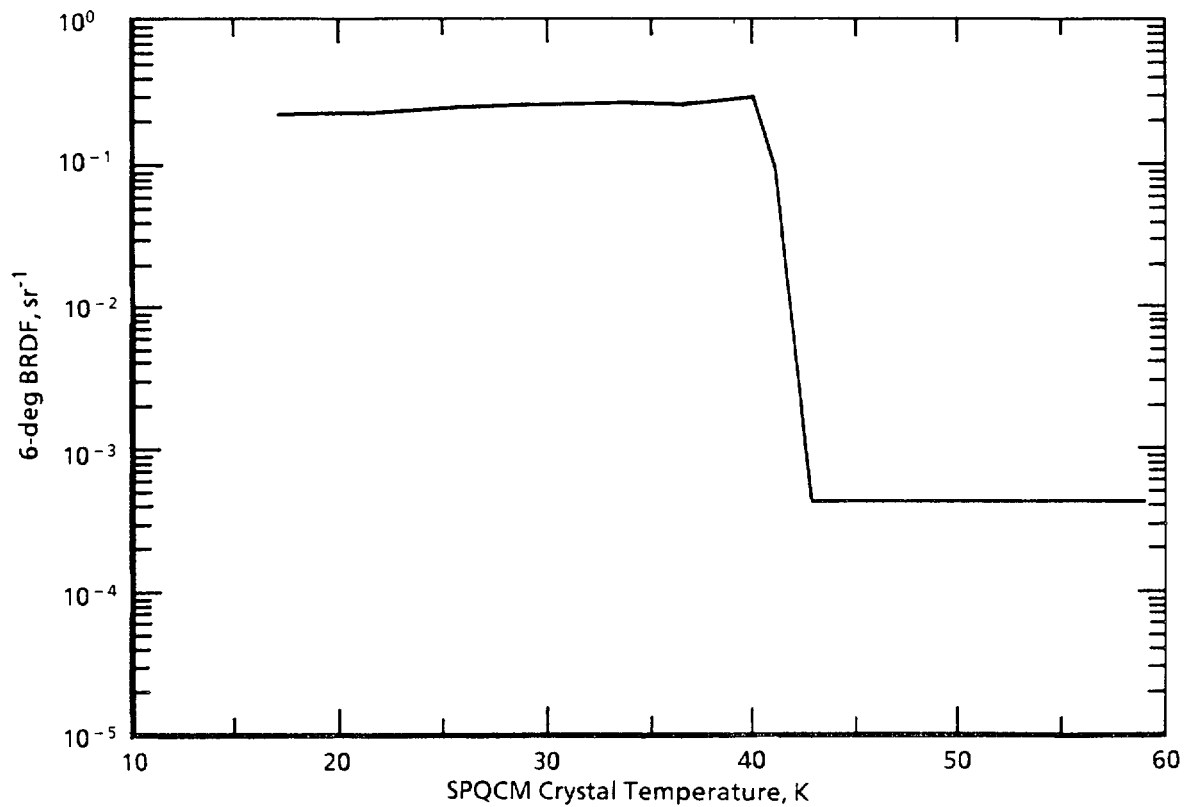
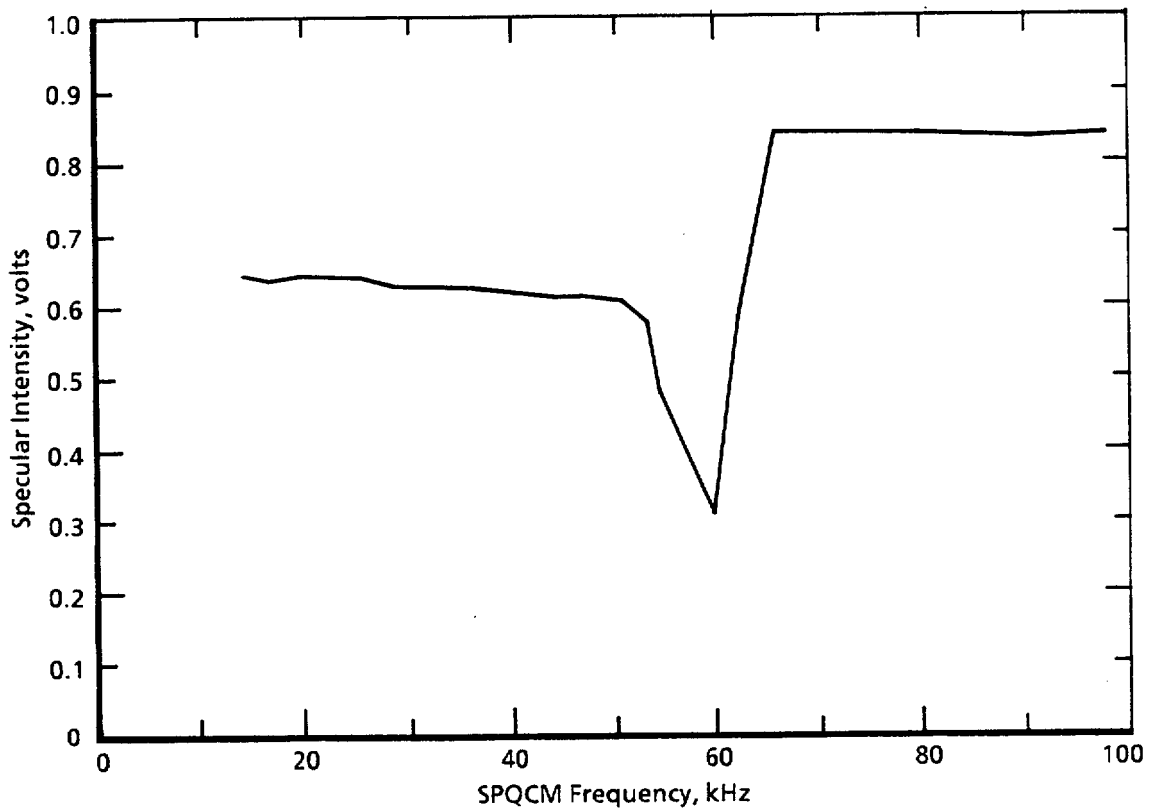


**Figure 10. Linearity of SPQCM frequency change with O<sub>2</sub> film thickness.**

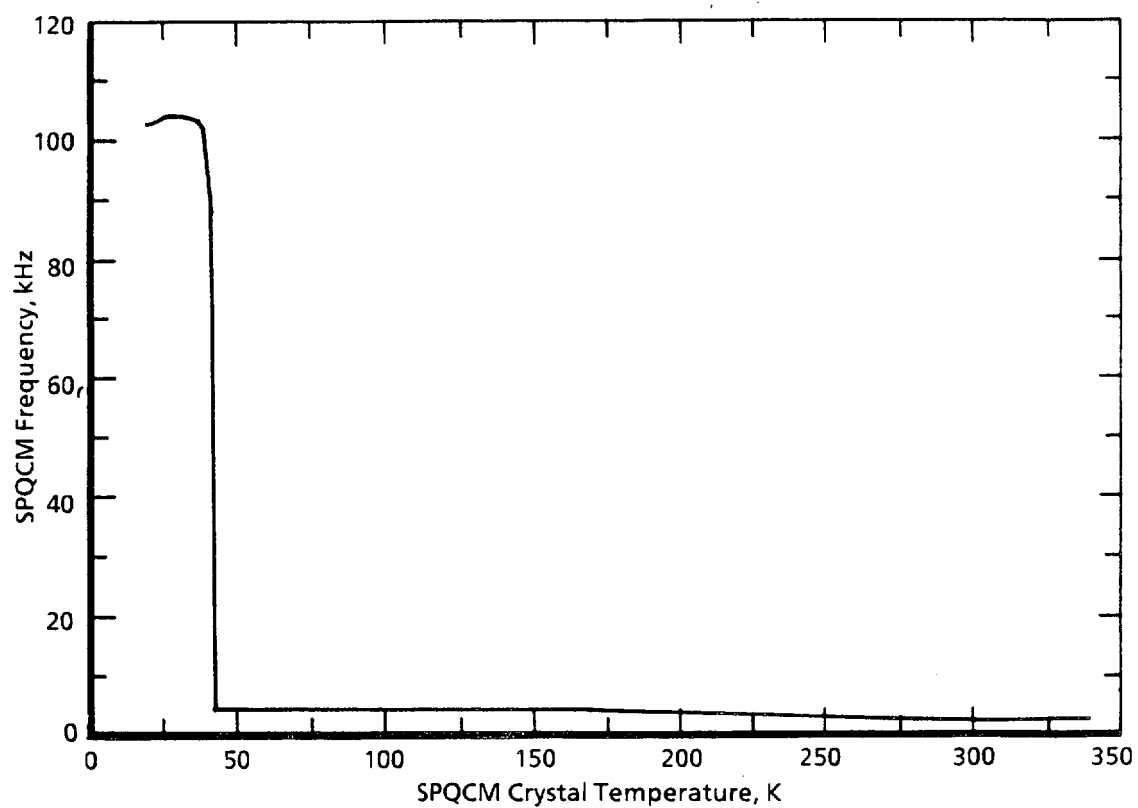


a. 6-deg BRDF with O<sub>2</sub> removal

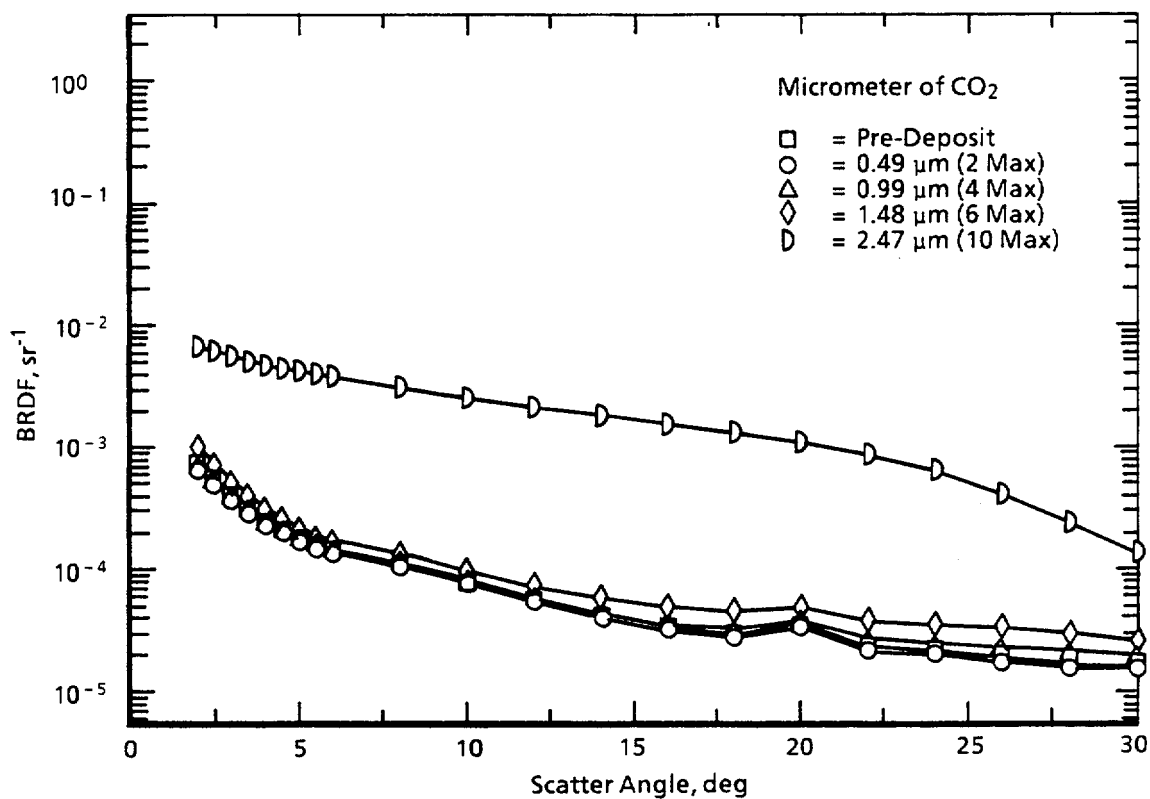
Figure 11. Warmup of SPQCM crystal with O<sub>2</sub> contaminant; 15 K surface, 0.6328  $\mu\text{m}$ .



**b. Specular intensity with O<sub>2</sub> removal**  
**Figure 11. Continued.**



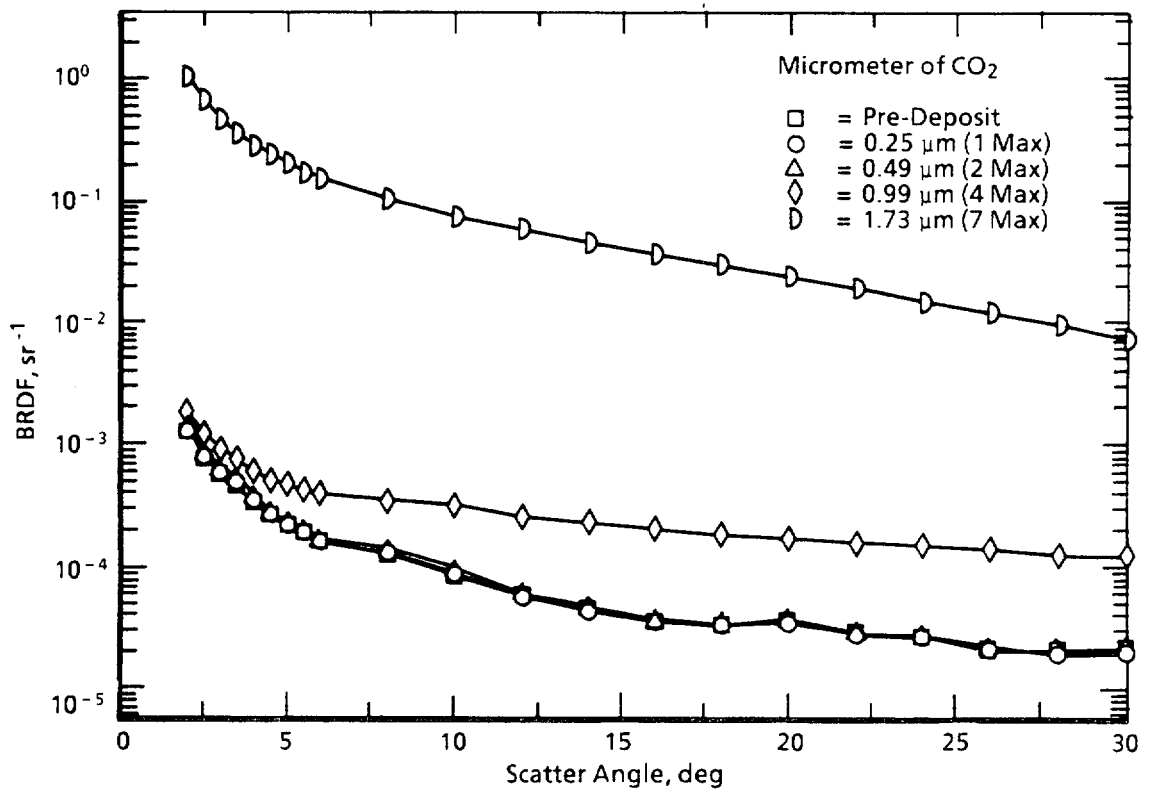
c. SPQCM frequency with O<sub>2</sub> removal  
Figure 11. Concluded.



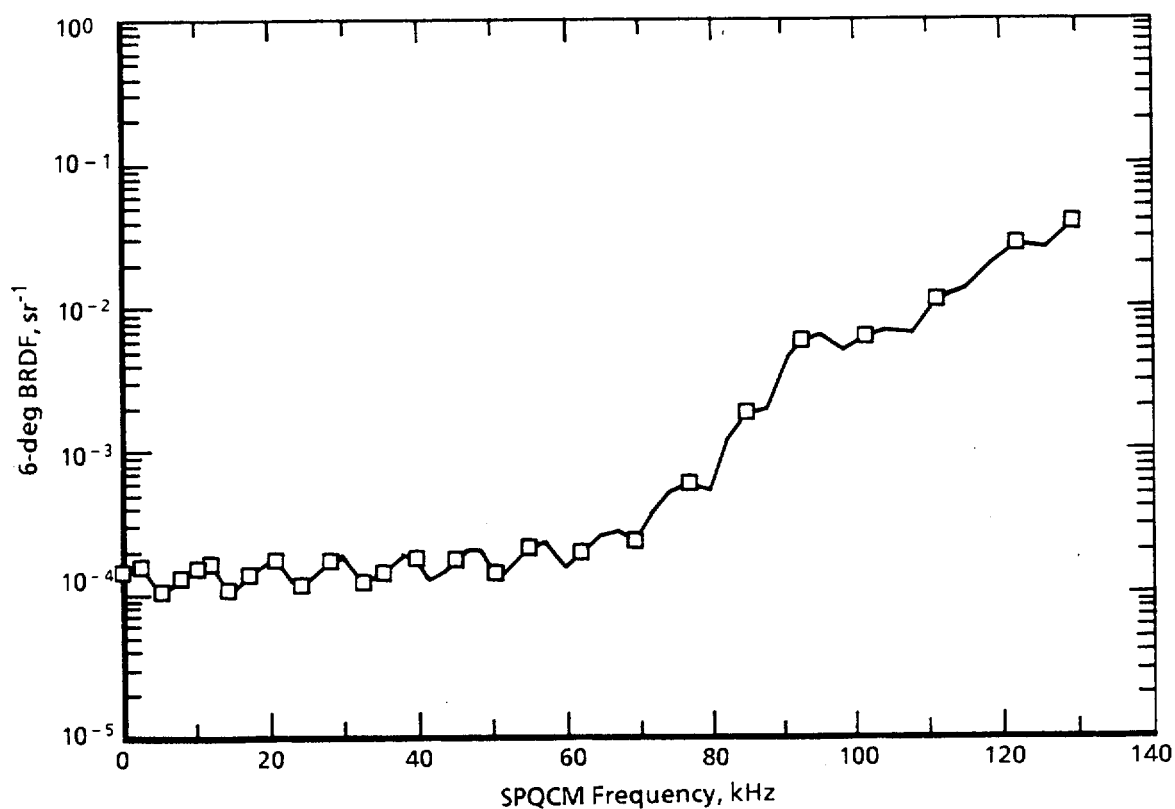
a. First run, 20 K surface

Figure 12. SPQCM degradation at selected CO<sub>2</sub> film thickness, 0.6328 μm.



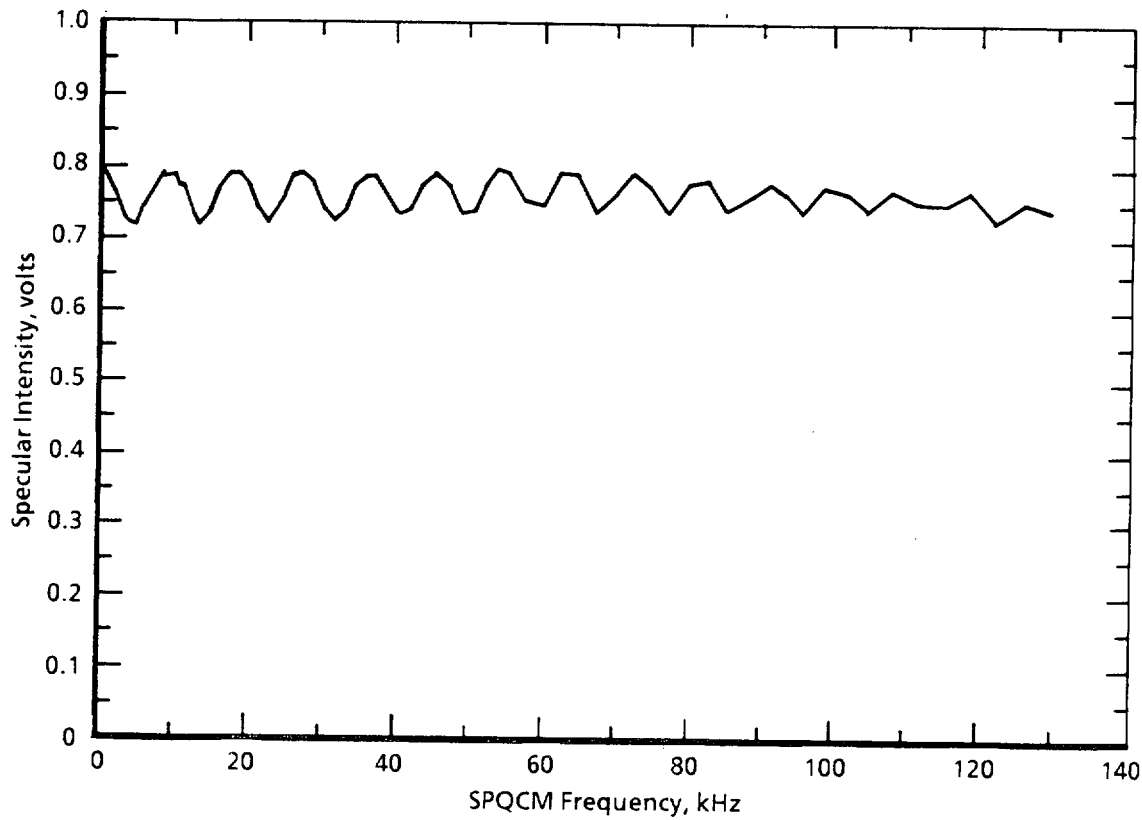


b. Repeat  $\text{CO}_2$  run, 15 K surface  
Figure 12. Concluded.



a. Effect of CO<sub>2</sub> on 6-deg BRDF

Figure 13. SPQCM with CO<sub>2</sub> contamination; 20 K surface, 0.6328  $\mu\text{m}$ .



**b. Effect of CO<sub>2</sub> contamination on specular intensity**  
**Figure 13. Concluded.**

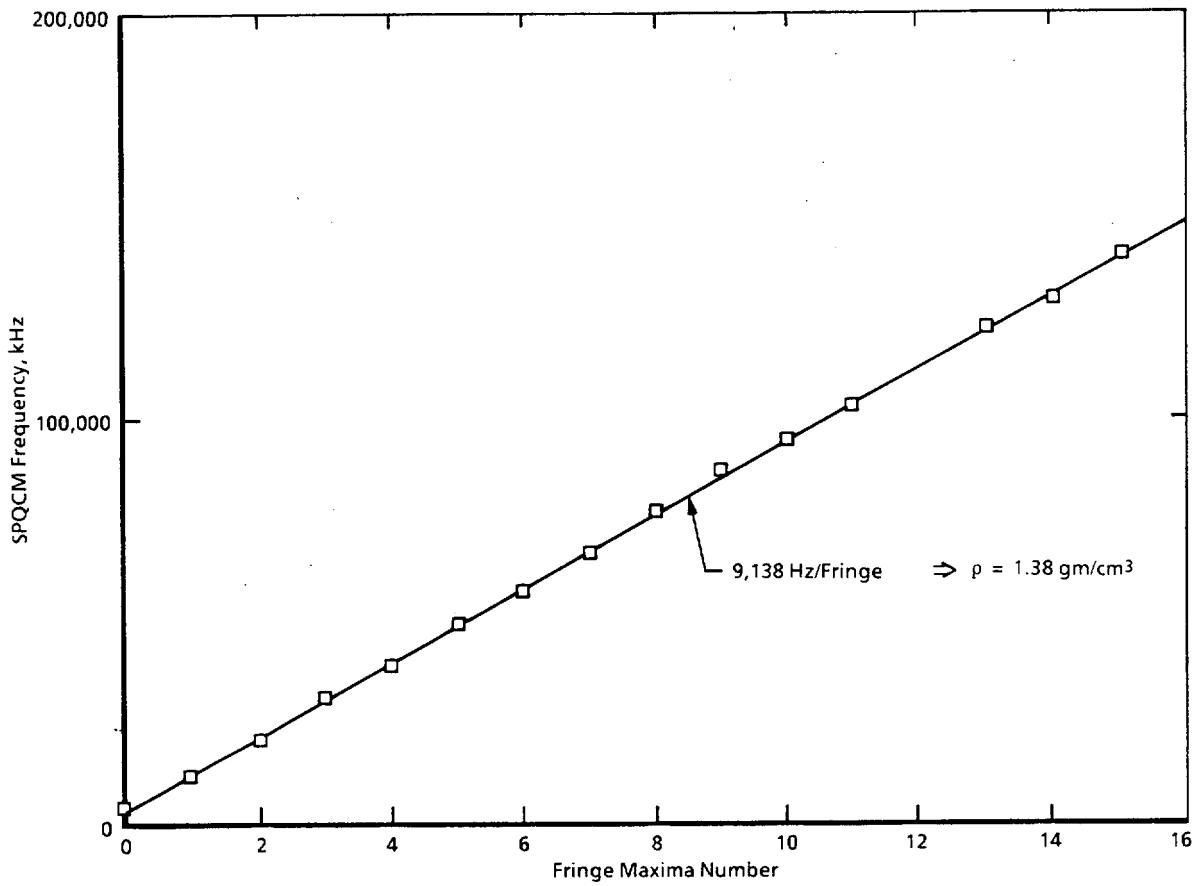


Figure 14. Linearity of SPQCM frequency with CO<sub>2</sub> film thickness.

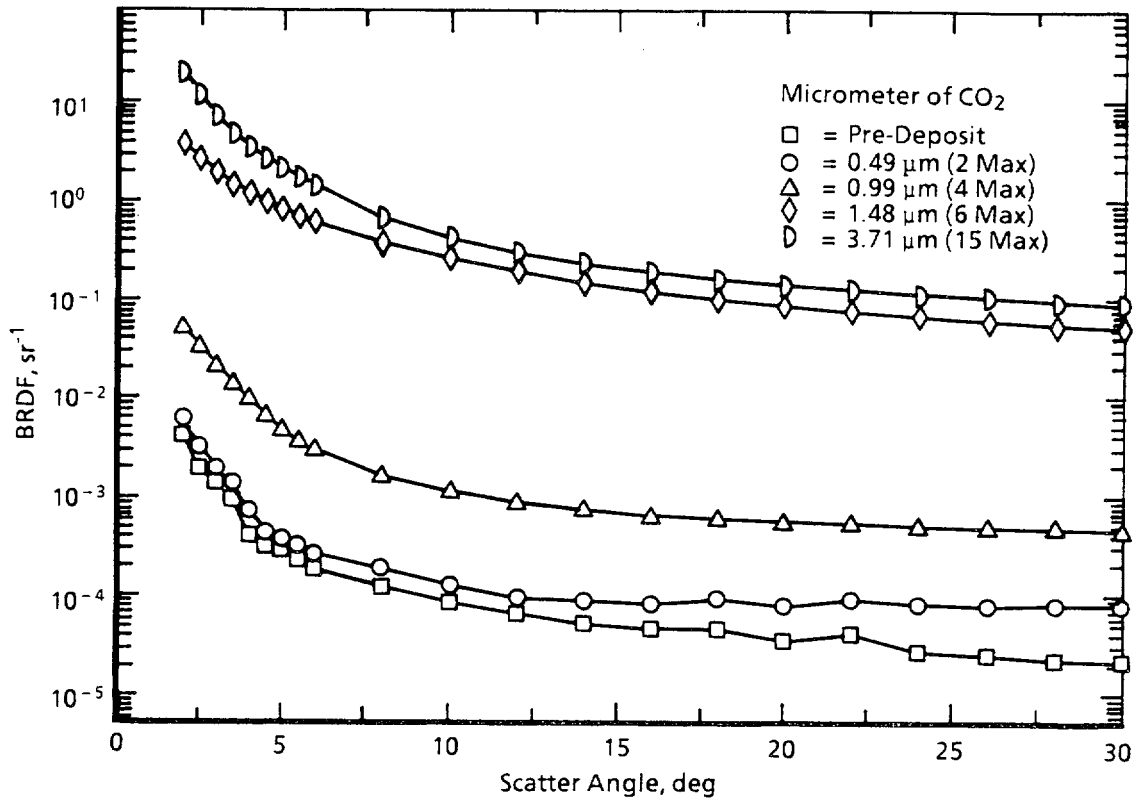


Figure 15. SPQCM degradation at selected H<sub>2</sub>O film thickness; 27 K surface, 0.6328 μm.

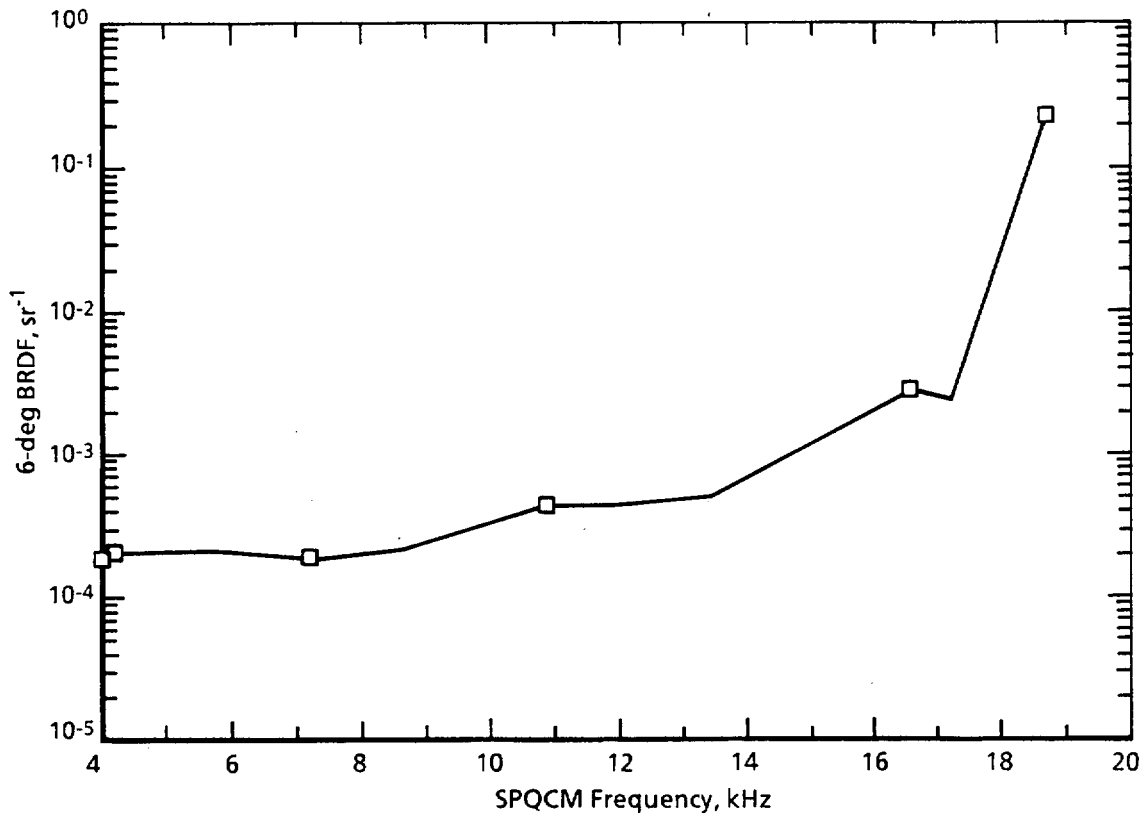
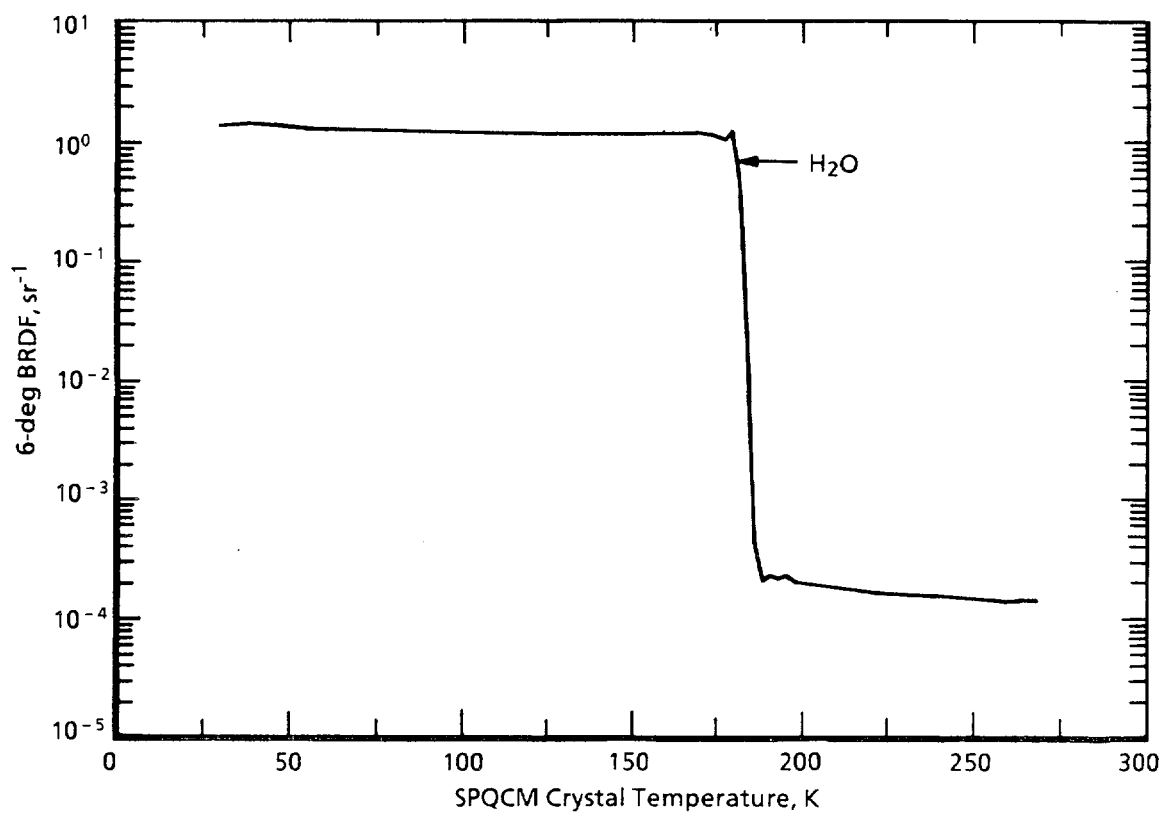


Figure 16. SPQCM 6-deg BRDF change with H<sub>2</sub>O contamination; 27 K surface, 0.6328  $\mu\text{m}$ .



**Figure 17. Change in 6-deg BRDF with SPQCM warmup; H<sub>2</sub>O contaminant, 27 K surface, 0.6328  $\mu$ m.**

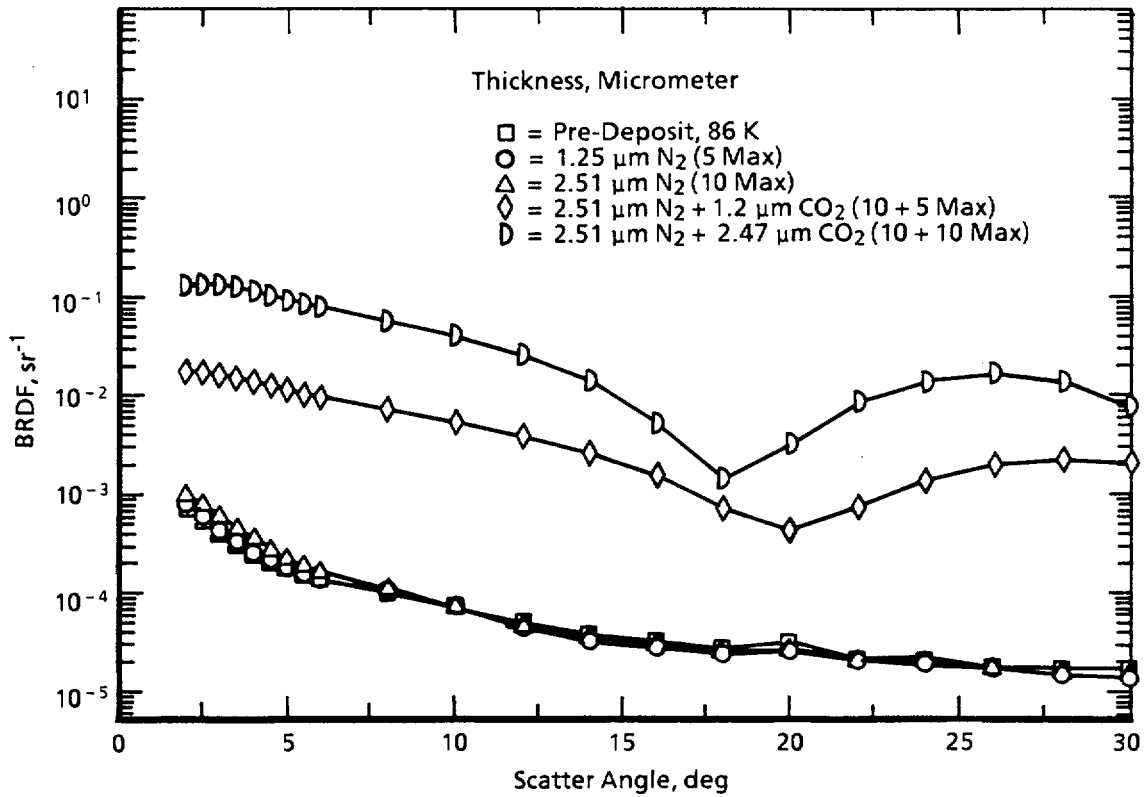
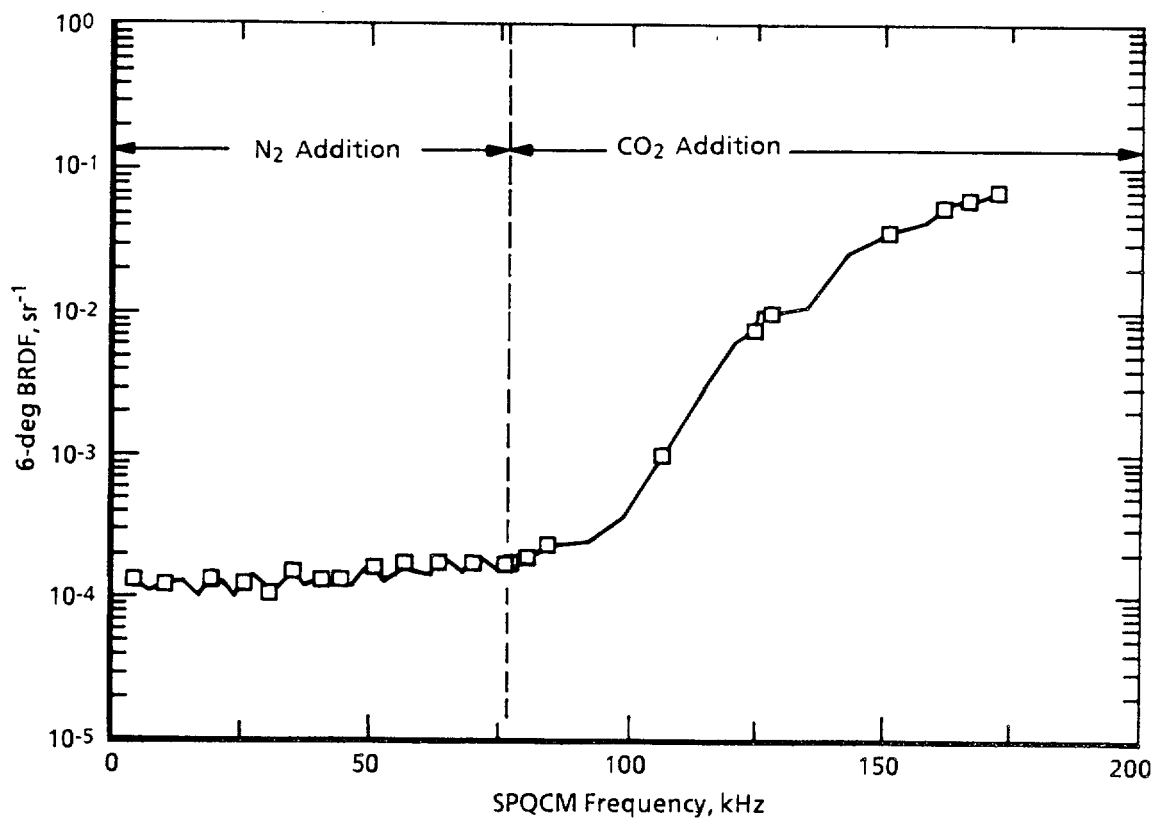


Figure 18. SPQCM degradation with film layers,  $\text{N}_2$  then  $\text{CO}_2$ ; 16 K surface, 0.6328  $\mu\text{m}$ .





**Figure 19. SPQCM 6-deg BRDF change with N<sub>2</sub> then CO<sub>2</sub> contamination layers; 15 K surface, 0.6328  $\mu$ m.**

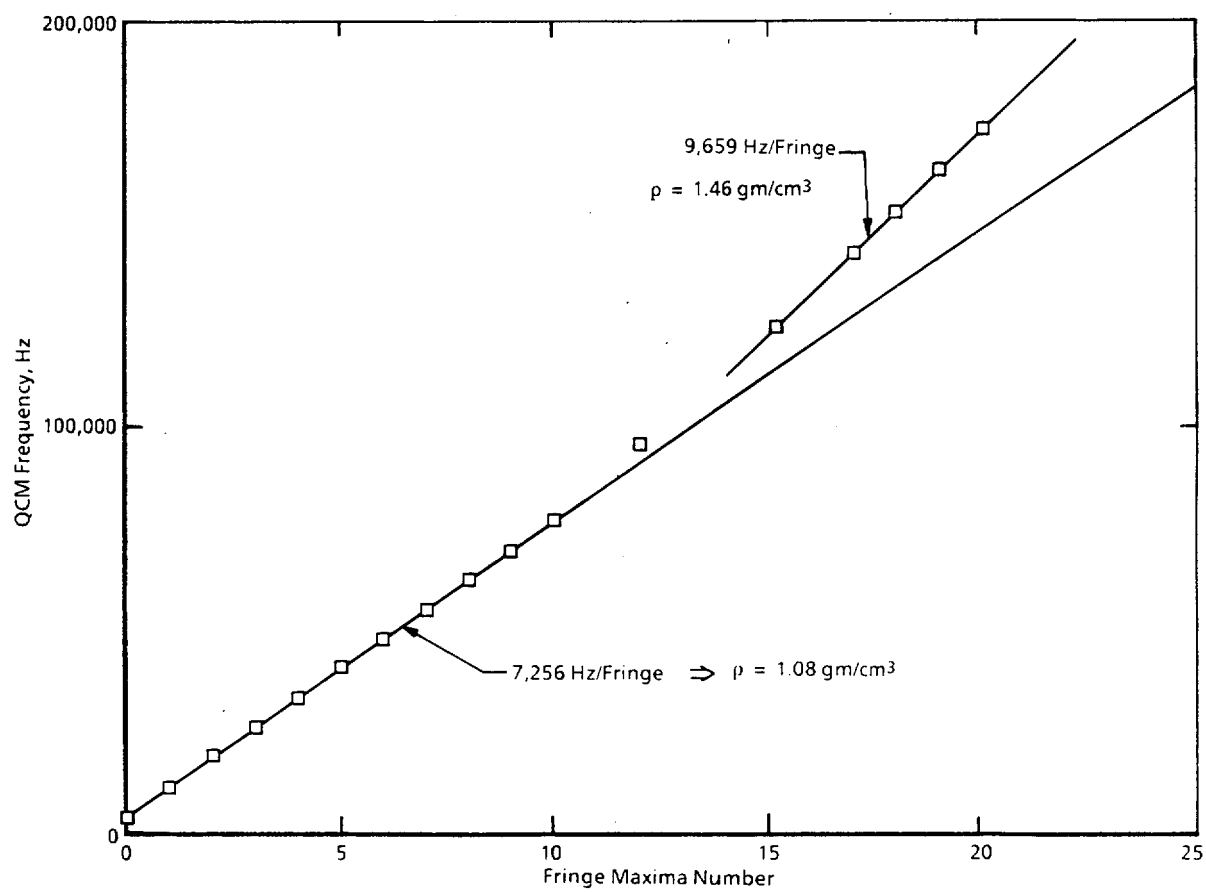
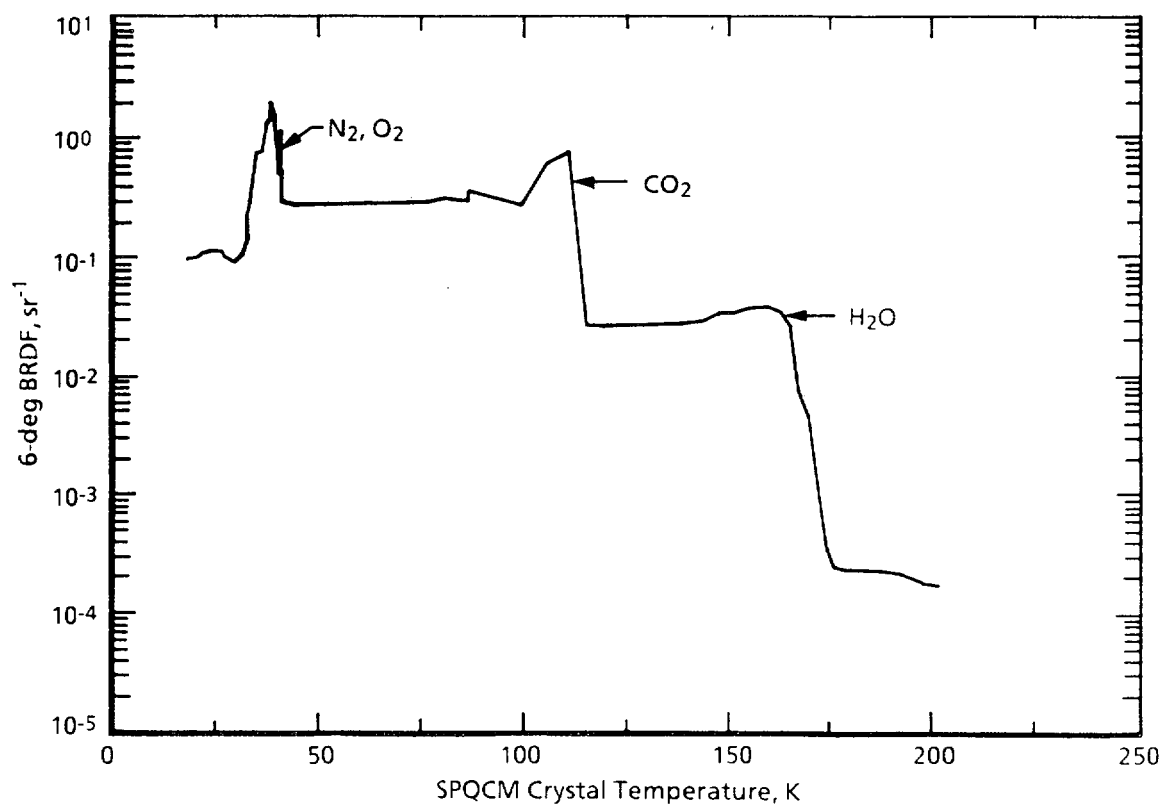


Figure 20. Linearity of SPQCM with layered film thickness, N<sub>2</sub> then CO<sub>2</sub>.



**Figure 21. Change in 6-deg BRDF with SPQCM warmup; contaminant, layered CO<sub>2</sub> over N<sub>2</sub>, 15 K surface, 0.6328  $\mu$ m.**

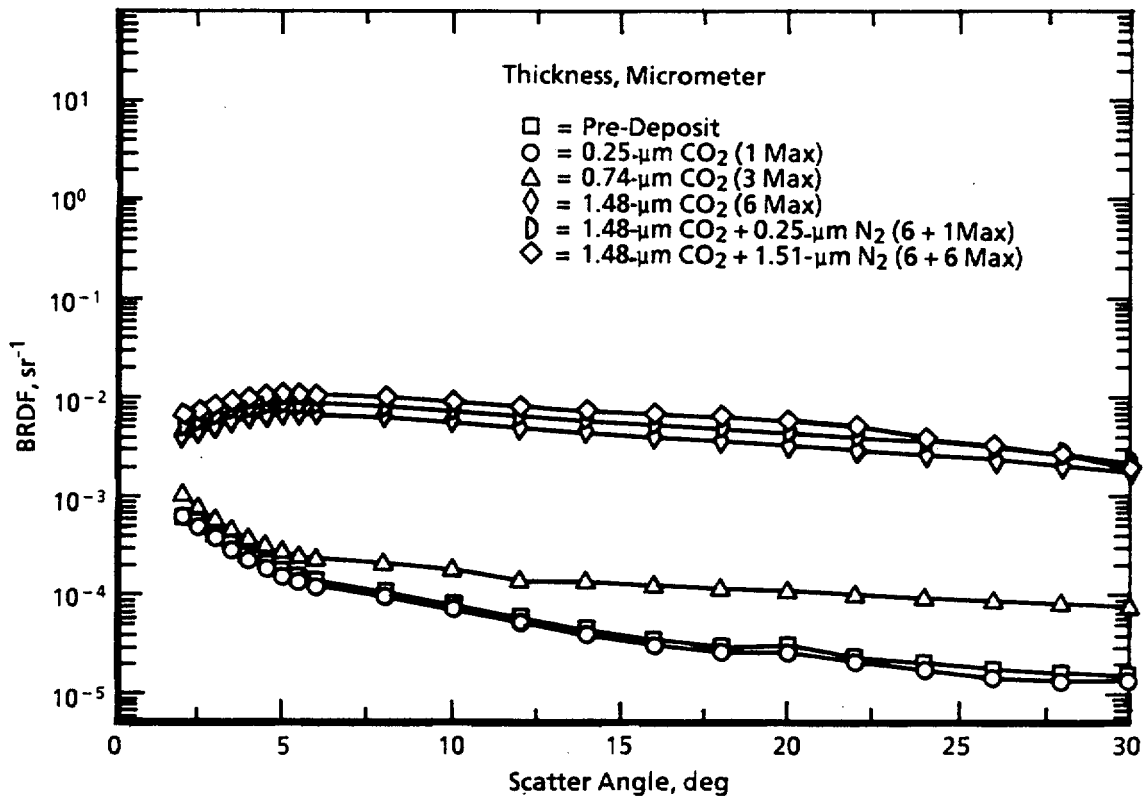


Figure 22. SPQCM degradation with film layers, CO<sub>2</sub> then N<sub>2</sub>; 15 K surface, 0.6328  $\mu\text{m}$ .

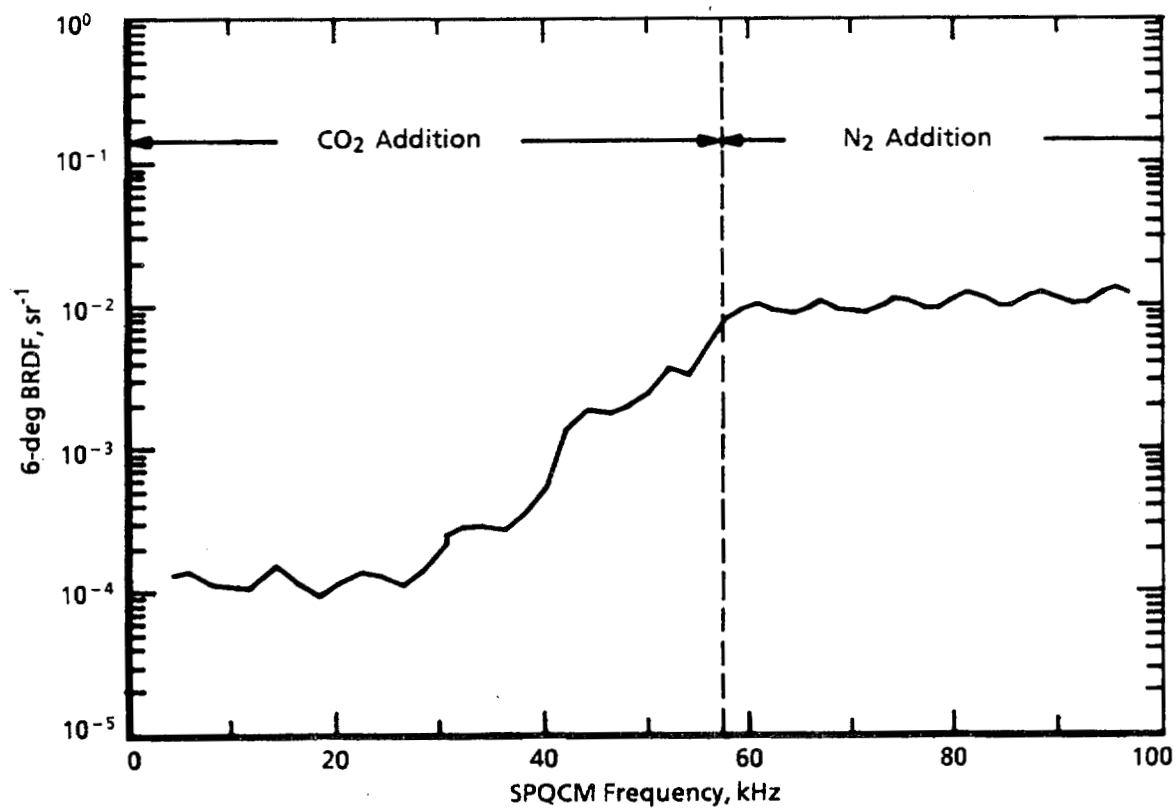


Figure 23. SPQCM 6-deg BRDF change with CO<sub>2</sub> then N<sub>2</sub> contamination layers; 15 K surface, 0.6328  $\mu\text{m}$ .

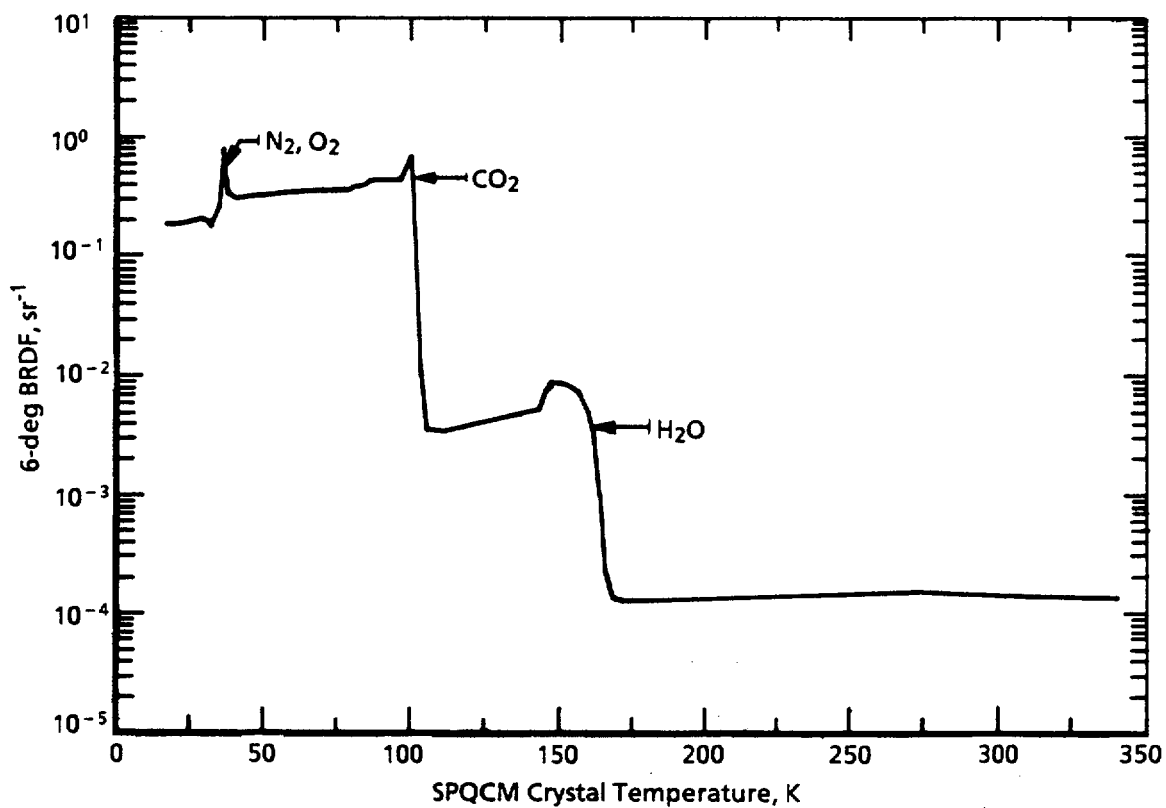


Figure 24. Change in 6-deg BRDF with SPQCM warmup; contaminant layered N<sub>2</sub> over CO<sub>2</sub>, 15 K surface, 0.6328  $\mu$ m.

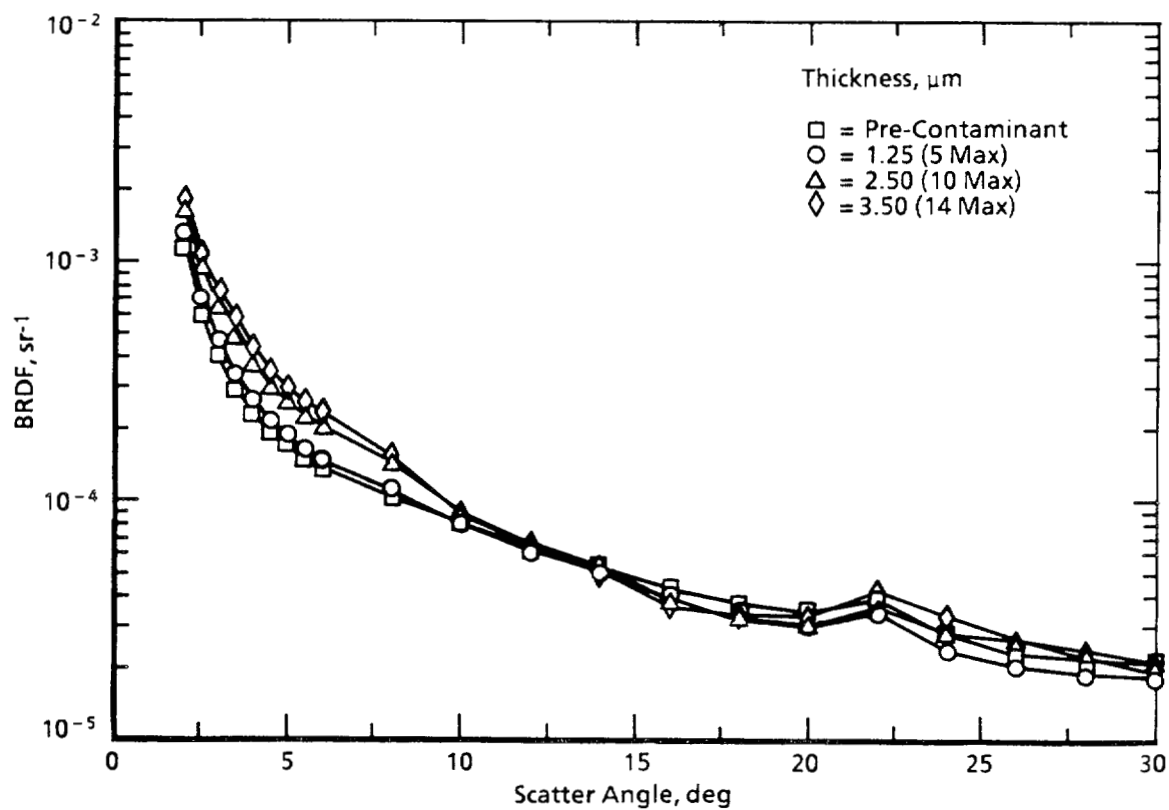


Figure 25. SPQCM degradation with film thickness; mixed gas with equal parts  $\text{N}_2$ ,  $\text{O}_2$ , and  $\text{CO}_2$ ; 16 K surface,  $0.6328 \mu\text{m}$ .

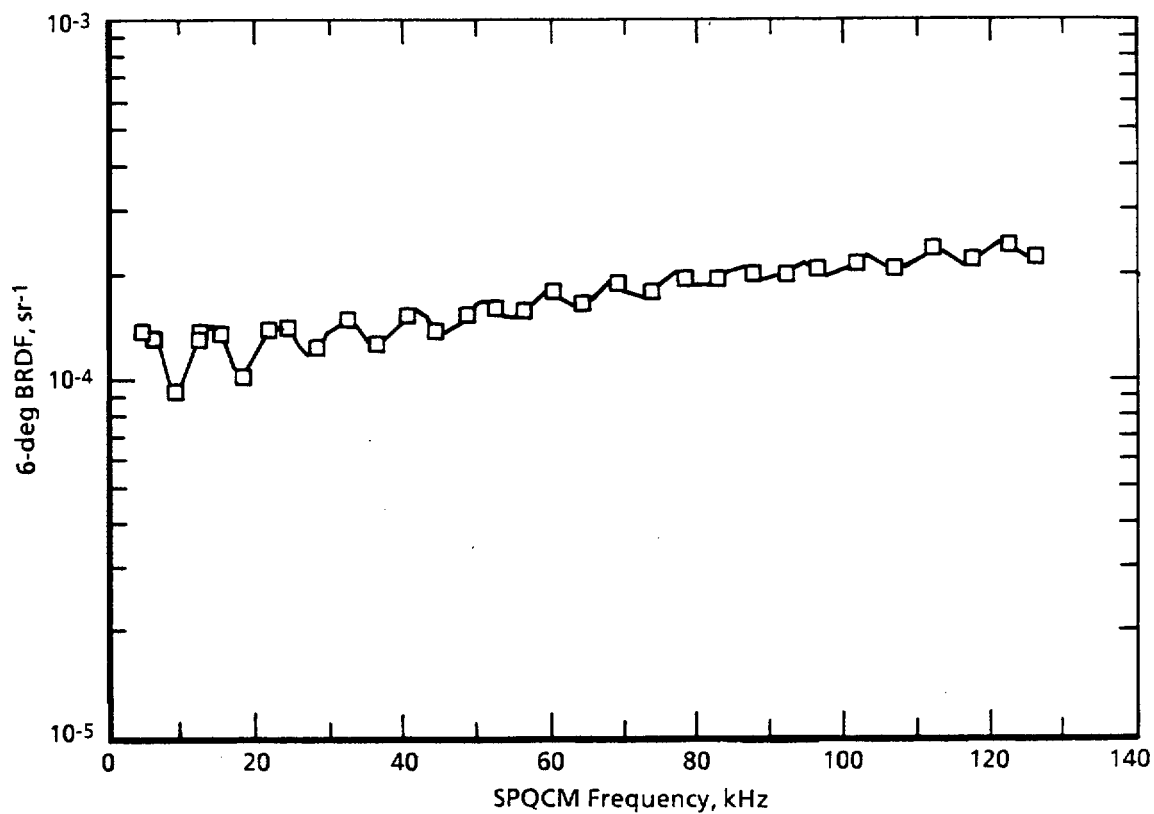


Figure 26. SPQCM 6-deg BRDF change with mixed gas contamination, equal parts N<sub>2</sub>, O<sub>2</sub>, and CO<sub>2</sub>; 16 K surface, 0.6328  $\mu$ m.